Slab-derived origin of tremolite-antigorite veins in a supra-subduction ophiolite; the Peridotite Nappe (New Caledonia) as a case study.

Dominique Cluzel, Philippe Boulvais, Marion Iseppi, Didier Lahondère, Stephane Lesimple, Pierre Maurizot, Jean-Louis Paquette, Alexandre Tarantola, Marc Ulrich

Slab-derived origin of tremolite-antigorite veins in a supra-subduction ophiolite; the Peridotite Nappe (New Caledonia) as a case study.

Cluzel Dominique[1], Boulvais Philippe[2], Iseppi Marion[1-3-4], Lahondère Didier[3], Lesimple Stéphane[4], Maurizot Pierre[4], Paquette Jean-Louis[5], Tarantola Alexandre[6], Ulrich Marc[7].

[1] University of New Caledonia, Institut des Sciences Exactes et Appliquées, BP R4 Nouméa, New Caledonia ; dominique.cluzel@unc.nc

[2] University of Rennes 1, CNRS UMR 6118, Geosciences Rennes, France

[3] Bureau de Recherches Géologiques et Minières, Orléans, France

[4] New Caledonia Geological Survey, DIMENC, Noumea, New Caledonia

[5] University Clermont-Auvergne, CNRS, IRD, OPGC, Laboratoire Magmas et Volcans, F-63000 Clermont-Ferrand, France

[6] University of Lorraine, CNRS, GeoRessources, Faculté des Sciences et Technologies, F-54506 Vandoeuvre-lès-Nancy, France

[7] University of Strasbourg, IPGS-EOST, CNRS UMR 7516, Strasbourg, France

Abstract

Hydration of mantle peridotites provides information on the exhumation history and on the fluid regime accompanying exhumation of these rocks (reservoirs involved, fluid/rock ratios, temperature of interaction). Highly depleted harzburgites and dunites of the Peridotite Nappe of New Caledonia are crosscut by fractures, which have been pervasively serpentinized, producing lizardite, brucite, magnetite and minor chrysotile in a near-static environment, probably by sea water circulating in cooling joints. This event is generally referred to as "primary serpentinization". In a next step, already serpentinized joints were re-opened to produce tension and shear cracks sealed by higher-temperature synkinematic fibrous minerals. Locally, tremolite-bearing veins and pockets, which do not display evidence for void infill, were generated by metasomatic replacement of the wall rock peridotite. Most veins only contain fibrous antigorite but some display tremolite-antigorite intergrowths or even pure tremolite. The latter rocks yield high contents of Ca and incompatible elements, which contrast with the overall depletion of the peridotite host rock and suggest contribution of an external source. Whole-rock geochemical and isotopic features ($^{87}Sr/^{86}Sr$, $\delta^{18}O$ and δH) suggest that antigorite veins, which bear highly radiogenic Sr isotope signatures, were strongly influenced by fluids emitted by the subducted slab and associated sediments. In contrast, the geochemical and isotopic signatures of tremolite-bearing rocks suggest a genetic link with Early Eocene supra-subduction dykes and fluids that leached them. Calcium, strontium and REE-bearing oxidized fluids reacted with already serpentinized fracture wall rock as shown by fibre nucleation, chromite alteration and high Cr contents in tremolite. The bulk of syn-tectonic fluid-rock interaction associated with shear and tensile fracture development probably occurred at the onset of Eocene intra-oceanic subduction, when the buoyant lower plate (the South Loyalty Basin) obliquely forced its way beneath the nascent Loyalty fore-arc. Mobile elements extracted from supra-subduction dykes temporarily enriched the circulating fluids and generated tremolite, antigorite, Mg-chlorite and magnetite instead of antigorite and magnetite solely. Tremolite crystallization probably ceased due to the exhaustion of Ca-rich fluids in a globally cooling fore-arc environment.

Keywords

Ophiolite, tremolite, antigorite, veins, metasomatism, supra-subduction, dykes

1. Introduction

Most ultramafic ophiolites are interpreted to represent supra-subduction mantle (Pearce et al. 1984) having recorded multiple events related to oceanic accretion, cooling, basin inversion and fore-arc evolution. Fluid and melt release through dehydration, decarbonation and partial slab melting within subduction zones is responsible for profound modifications of the supra-subduction mantle, which are overprinted on previous metasomatic events. Hydration of supra-subduction mantle peridotites (Wang et al. 2009; Mothersole et al. 2017) results in the occurrence of hydrous silicates of the serpentine and amphibole groups, which are difficult to distinguish from those formed near the ridge during the cooling of the ocean lithosphere (Mével 2003; Morishita et al. 2009). In contrast, melts appearing during the early stages of arc formation (fore-arc melts) display diagnostic features that may be a clue for identifying supra-subduction events.

The ultramafic allochthon of New Caledonia, termed Peridotite Nappe (Avias 1967; Fig. 1), is formed of partly or totally serpentinized peridotites, which have evolved from a back-arc basin ridge into a fore-arc setting, before being obducted (Cluzel et al. 2012). The Peridotite Nappe is crosscut by a spaced vein network, which contains fibrous minerals that mainly belong to the serpentine group (antigorite, chrysotile) and more rarely to the amphibole group (anthophyllite, tremolite). Most antigorite and tremolite occurrences correspond to synkinematic fibrous seals associated with the opening of tension cracks, or motion along micro-faults. However, some tremolite occurrences appear in irregular streaks and pockets without obvious link to faults, and partly correspond to metasomatized peridotites, which contain remains of their protolith such as chromite streaks (Lahondère et al. 2012).

In weakly serpentinized lherzolites of the Peridotite Nappe, calcium content is relatively high (1.5 wt% to 2.2 wt% CaO) (Secchiari et al. 2016). It is lower in unserpentinized harzburgites (0.3 wt% to 0.6 wt% CaO) (Secchiari et al. 2019). However, occurrence of such fresh rocks is extremely rare and the bulk of the Peridotite Nappe underwent 40% to 100% serpentinization (lizardite mesh) and contain less than 0.1 wt% CaO (0.01%-0.1%), a general feature of serpentinized peridotites (Kodolànyi et al. 2000). In spite of this, tremolite, a Ca-rich amphibole, is not unusual in serpentinized ultramafic rocks and occurs in tectonic melanges, unroofed abyssal peridotites, transform fault zones and fore-arcs (e.g., Kodolànyi et al. 2000). Tremolite occurrences and hence Ca input have been attributed to mobilization from the peridotite itself or, alternatively, external sources. As far as an external source is needed, tremolite crystallization may result from the interaction of serpentinite with Ca-rich metasediments in mélanges (i.e., nephrite jade; Adams et al. 2007) or with mafic rocks in subduction zones (Marocchi et al. 2010), from the recrystallization of dykes crosscutting serpentinites (e.g., rodingites; Bach and Klein 2009; Harlow and Sorrensen 2005; Koutsovitis et al. 2013; Sivell and Waterhouse 1986), from mobilization of Ca from pyroxenes during serpentinization (Python et al. 2011), or "hydrothermal" remobilisation of Ca from calcite veins coming from sea

water at shallow depth (Agrinier et al. 1996). In New Caledonia, in addition to crosscutting veins, tremolite locally appears in the lower crustal section of the Peridotite Nappe in greenschist-facies mylonitic gabbronorite cumulates (Ouen Island "jade"; Maurizot and Lesimple 2012). However, in these rocks tremolite displays strong preferred orientation but never shows asbestiform texture. In contrast, tremolite occurrences dealt with in this article are always located in serpentinized peridotite, away from any mafic crustal rock.

In a general fashion, fibrous crack seals are nucleated on wall rock and the nature of minerals that fill the progressively opening spaces depends strongly on the composition of the host rock. There is a consensus on the fact that synkinematic minerals, which form the crack seals, come from pressure- or shear-solution and are in equilibrium with pore fluids. Thus, synkinematic mineral growth is at least partly fed by dissolved elements that are not carried over large distances (e.g., Baghat and Marshak 1990; Beach 1974, 1977; Bons and Jessel 1997; Durney 1972, 1976; Pollard and Segall 1987; Rutter 1983). Accordingly, only serpentine minerals (antigorite, lizardite, chrysotile, polygonal serpentine, depending upon P-T conditions) are expected to be in equilibrium with the more or less deeply serpentinized peridotite wall rock. This assertion has been confirmed by recent studies (Andreani et al. 2007; Kurat et al. 2011); therefore, owing to the very low Ca content of depleted peridotite, the occurrence of faults and cracks filled with tremolite in the Peridotite Nappe raises the question of the composition and the origin of the associated fluids.

No associated sediments are known in the Peridotite Nappe that could be a source for Ca. Scarce carbonate veins are documented in the Peridotite Nappe (e.g. Lahondère et al. 2012; Mothersole et al. 2017) and clearly post-date the bulk of serpentinization. Generally these veins are composed of magnesite or hydromagnesite, and although aragonite has been observed locally (Lahondère et al. 2012) it is related to late (post-obduction ?) joints infill of supergene origin.

Therefore, there are three internal and external possible sources:

i. Calcium may come directly from fluids emitted by the subduction zone.

ii. Although harzburgites and dunites of the Peridotite Nappe are strongly depleted (even unserpentinized rocks -a very rare occurrence though- yield very low Ca contents), they could be a source of Ca for tremolite, provided the leaching of large amounts of rock.

iii. Early Eocene felsic dykes (up to 17 wt% CaO; Cluzel et al. et al. 2006) emplaced in already fractured and serpentinized rocks commonly display disequilibrium features related to syn- and post-magmatic tectonics (Rodgers, 1973a, b, 1974; Cluzel et al. 2006; see below), which suggest easy fluid circulation through the fracture network and a possible source for Ca.

Tracking the origin of the tremolite-crystallizing fluids has been attempted using four methods: i) geological characterization of the geometry and kinematics of the veins; ii) major elements, trace elements, and REE geochemistry of tremolite-bearing veins; iii) Sr isotopes (tracer of Ca origin); and

iv) oxygen ($^{18}O/^{16}O$) and hydrogen (D/H) isotope ratios. As far as possible, tremolite features have been compared with that of fibrous minerals of the serpentine group (antigorite), which are commonly associated with tremolite in peridotite massifs.

2. Geological setting

The geology of New Caledonia is characterized by: i) a pre-Late Cretaceous basement formed of amalgamated arc-derived terranes (Meffre 1995), which relate to the Southeast Gondwana margin; ii) a Late Cretaceous to Late Eocene sedimentary cover; iii) a Eocene high-pressure metamorphic belt, exposed in the northern part of the island; and, iv) two large allochthonous terranes emplaced during the Eocene, the Poya Terrane and the Peridotite Nappe, which together represent almost one half of the island's surface (Fig. 1) (Cluzel et al. 2012; Maurizot et al. in press a).

The Peridotite Nappe of New Caledonia (Avias 1967), results from obduction of the Loyalty Basin lithosphere over the continental Norfolk/New Caledonia Ridge (Collot et al. 1987). It originally covered most of the island; however, several phases of erosion isolated tectonic klippes spread along the west coast and a larger unit termed "Massif du Sud" in the south of the island. A highly sheared serpentinite sole, 20-200 m thick, indicates top-to-the-southwest emplacement kinematics (Quesnel et al. 2013, 2016), while thrust-related deformation rapidly decreases upward.

The Peridotite Nappe is dominantly composed of harzburgite (>80%), dunite and minor lherzolite (in northern massifs only) that represent a prominently depleted supra-subduction mantle lithosphere (Marchesi et al. 2009; Pirard et al. 2013). Owing to their depletion in incompatible elements compared to primitive mantle composition, residual harzburgites probably underwent about 20%-25% partial melting (Prinzhoffer 1981; Secchiari et al. 2019). They are overlain by dunite, pyroxenite, websterite and gabbronorite cumulates (Prinzhoffer 1981). Cumulate websterite and gabbronorite probably crystallized in equilibrium with depleted melts intermediate between boninite and island-arc tholeiite (Marchesi et al. 2009; Pirard et al. 2013; Cluzel et al. 2016; Secchiari et al. 2018), which at present are not preserved. Whole rock and mineral chemical constraints on lherzolites allow a polyphase evolution to be drawn, from re-enrichment by circulating melts during oceanic accretion to mantle metasomatism during subduction (Marchesi et al. 2009; Secchiari et al. 2016; Spandler and Pirard 2013; Ulrich et al. 2010).

The inception of intra-oceanic subduction that eventually led to obduction is time-constrained by the granulite-facies "metamorphic sole", dated at 56 Ma (Cluzel et al. 2012a). Afterwards, the Peridotite Nappe was crosscut by a series of dykes and sills emplaced at ca. 55-50 Ma (Early Eocene; Cluzel et al. 2006), which are not present in the underlying Poya Terrane. These intrusive rocks comprise minor dolerite dykes, and a variety of medium to coarse grain rocks (sills and dykes), the compositions of which vary from ultramafic (pyroxenite and hornblendite) to felsic (diorite,

leucodiorite and granite). Dolerite dykes crosscut all the levels of the Peridotite Nappe, including gabbro cumulates, while felsic and intermediate dykes and sills are apparently restricted to the ultramafic part of the allochthon. Dolerites display supra-subduction affinities (island-arc tholeiites), and likely represent the product of partial melting of "normal" supra-subduction mantle. In contrast, the majority of felsic or intermediate dykes come from slab melts formed by partial melting of diverse mafic oceanic crust rocks including gabbro cumulates; some others, however, may be referred to as boninite-series generated by hydrous melting of highly depleted mantle wedge peridotites enriched by slab melts and fluids (Cluzel et al. 2006, 2016; Secchiari et al. 2018).

Thin tremolite coatings around high-temperature minerals (olivine/orthopyroxene) and crosscutting tremolite needles, which have been rarely found in unserpentinized harzburgites (Secchiari 2016; Secchiari et al. 2019), signal early Ca input by circulating fluids or melts. Rocks of the Peridotite Nappe are serpentinized at various degrees (0% to 100%) and this early tremolite crystallization did not survive the development of lizardite-brucite (± chrysotile) mesh and tremolite now only appears in syntectonic or replacement veins in serpentinized peridotites.

The development of serpentinization at large scale is crucial for Ni ore-forming processes during tropical weathering (e.g. Orloff 1968; Pelletier 1996; Butt and Cluzel 2013; Maurizot et al. in press b) because Ni substitutes Mg to form Mg-Ni silicates (the garnieritic ore) and has been systematically described by mining geologists. Since the work of Orloff (1968) in New Caledonia, there has been a consensus about the timing and origin of serpentinization, which was considered to be primarily related to Eocene obduction and decreasing in intensity from the serpentinite sole upwards. However, this view, which fits well with serpentinization at a large scale, is challenged by the local observations of unserpentinized peridotites in which incipient serpentinization develops downwards independently of the distance to the tectonic sole.

Thus, three main episodes of serpentinization may be defined: i) primary (intra-oceanic) serpentinization is thought to have formed during cooling and hydration of mantle lithosphere; ii) secondary, upward decreasing serpentinization was likely due to the subduction/obduction process; iii) finally, continuing (minor?) serpentinization accounts for the local occurrence of hyper-alkaline springs (Monin et al. 2014), somewhat similar to the Lost City oceanic geothermal field (Rivizzigno et al. 2001). The products of present serpentinization are unknown and could only be reached by drilling.

Serpentines formed by "primary" serpentinization and that due to subduction/obduction are dominated by lizardite and somewhat difficult to discriminate where they overprint each other. The only difference holds in the large amount of chrysotile, which is apparently a feature of the tectonic sole.

With the exception of the tectonic sole, the Peridotite Nappe is weakly deformed and displays m- to dm-spaced joints with only scarce evidence for shearing motion. Most of these joints have

serpentinized boundaries mm- to dm-thick, composed of sheeted seams of dark cryptocrystalline lizardite and brucite crosscut by minor chrysotile veins. From the serpentinized fractures outwards, lizardite seams are connected to the intra-crystalline serpentine mesh of olivine, which forms 40% to 100% of the bulk rock volume. In extremely scarce locations, peridotites have escaped pervasive serpentinization and allow the observation of its progressive development. These weakly serpentinized areas display upward, downward and laterally increasing amount of serpentinization without strong associated deformation. Fresh olivine grains are crosscut by closed micro-cracks (Fig. 2a), which probably resulted from cooling-related differential shrinkage. Interconnection of these micro-cracks with lizardite-bearing well-organized fractures (Fig. 2b) suggests that these structures have been controlled by larger-scale joint development (Fig. 2c & 2d). Serpentinization progressed from the fracture walls outward without significant relative motion and the occurrence of almost undeformed mineral grains such as pyroxene (bastite) or chromite forming bridges across the serpentinized fractures show that the latter were not significantly open and serpentinization was dominantly static. The process of serpentinization may have varied through time and from place to place and secondary minerals show some compositional variation due to protolith, fluid composition, temperature and variation of the fluid/rock ratio (for a review, see Agrinier et al. 1996; Frost et al. 2013 and references therein). It is worth noting that "primary" serpentinization (i.e. lizardite-forming) left chromite grains unaltered; in contrast, chromite grains in antigorite-tremolite veins frequently display chromian magnetite pseudomorphs (see below).

In contrast with static (or primary) serpentinization, which never gave birth to Ca-bearing silicates, the crystallization of fibrous antigorite (and minor chrysotile) and tremolite occurred when serpentinized fractures were reactivated by opening perpendicular or oblique to fracture walls filled with synkinematic fibrous minerals (Fig. 3). Antigorite-bearing veins are widespread in the Peridotite Nappe (e.g., Lahondère et al. 2012; Quesnel et al. 2016). They commonly reach several metres in length and bear fibrous crack seals several mm to dm long. The angle between fibres and vein walls is generally acute (45-25°) and denote oblique opening. Vein boundaries are generally composed of dark lizardite, on which antigorite fibres are nucleated (Fig. 3b); but in some other localities, the vein boundaries are made of porcelain-like whitish serpentine seams, which may result from the leaching or recrystallization of lizardite vein walls.

Antigorite-tremolite and pure tremolite veins display the same characteristics; however, tremolite fibres are shorter and commonly perpendicular or strongly oblique to vein walls (Fig. 3c & 3d). In all cases the development of antigorite and tremolite post-dated the lizardite-bearing "primary" serpentinization.

3. Analytical procedures

Because it may have fibrous, asbestiform habits (Dorling and Zussman 1987), and frequently shows intergrowth with antigorite (this study), tremolite was sometimes overlooked in the field. Therefore, lab analysis (i.e., polarized light microscopy, XRD, IRS, Raman spectrometry) was often necessary to distinguish the various asbestiform minerals.

Raman data were acquired with a Renishaw inVia spectrometer of the Geology Lab. of Ecole Normale Supérieure de Paris. The spectrometer is fitted with a Physics Argon laser delivering monochromatic coherent light beam of 20mW at 514.5 nm (green laser). The laser beam is focused through a Leica DMLM microscope fitted with 4 short focus lenses (x5, x20, x50 (Numerical aperture=0.75), x100 (NA=0.90)) and 2 long focus lenses (x50 and x100). In the most effective configuration, the resolution was in the order of 1µm for 1mW power at the sample surface so that any irradiation damage may be avoided. The Rayleigh diffusion (< 100 cm^{-1}) was eliminated by dielectrical filters. The Raman signal was then spread with a network of 1800 lines mm^{-1} (or 3000 lines mm^{-1}) and measured with a CCD RENCAM detector of 400 x 576 pixels cooled by Peltier effect. The microspectometer is fitted with a motorized Prior Scientific stage, which allowed moving across the sample

Geochemical whole-rock analyses were performed at Service d'Analyse des Roches et Minéraux (CNRS-CRPG, Vandoeuvre, France). Major elements were analysed by ICP-AES, trace and Rare Earth elements by ICP-MS (a description of analytical procedures and detection limits may be obtained on the SARM web site: http://helium.crpg.cnrs-nancy.fr/SARM/).

Single minerals major elements concentrations have been determined on polished thin sections with a Cameca SX five electron microprobe (W beam source) of the analytical platform of University of Orleans/CNRS/BRGM.

Strontium isotope analyses have been carried out at Clermont-Ferrand isotope laboratory of Laboratoire Magmas et Volcans (UMR 6524 CNRS-Université de Clermont-Ferrand, France) by TIMS using a Thermo Fischer Triton instrument, corrected for mass fractionation by normalisation to $^{86}Sr/^{88}Sr = 0.1194$. Strontium sample decomposition and chemical separation followed the procedure developed by Pin and Santos Zalduegui (1997). Strontium isotope ratios were corrected for in-situ decay at 53 Ma, based upon the average U-Pb zircon age of dykes (Cluzel et al. 2006). Concentrations of Sr are given in $\mu g.g^{-1}$. The $^{87}Sr/^{86}Sr$ ratio measured for the NIST SRM 987 standard during the period of analyses gave a mean value of 0.710238 ± 9 (2σ, n = 30).

Oxygen isotope compositions were measured on dried silicates reacted using BrF_5, following the method of Clayton and Mayeda (1963). Isotopic compositions were measured on CO_2 with a VG Optima triple collector mass spectrometer. Measured isotopic compositions were normalized to NBS 28 standard (9.6 ‰). The reproducibility is 0.25‰.

Hydrogen isotope compositions were analyzed at the CRPG UMR 7358 CNRS-UL (Nancy, France) using an Eurovector Elemental Analyzer (EA) coupled to a VG Isoprime Isotope Ratio Mass

Spectrometer (IRMS), following the procedure described in Lupker et al. (2012), Bell and Ihinger (2000) and Bigeleisen et al. (1952). Powdered samples were loaded into tin capsules and degassed at 120 °C under vacuum for 48 h in a degassing canister to remove adsorbed water. After dehydration, samples were transferred under a N_2 dry atmosphere in a customized, sealed, automatic sampler pre-flushed with He in order to avoid any contact with atmospheric moisture. This sampler was then connected to the EA-IRMS system. Samples were combusted at 1450 °C on an EA glassy Carbon reaction tube, filled with glassy carbon chips, leading to the reduction of hydroxyl groups to H_2. After chromatographic separation, the recovered H_2 was introduced in the IRMS source and analyzed for hydrogen isotopic composition. Three different internal standards (Muscovite: MuscD65, Phlogopite: Mica-Mg and a fine grained marine sediment from the Bay of Bengal: SO188) were included during the sample analyses. Values of δD are reported in standard per mil (‰) notation relative to SMOW (Standard Mean Ocean Water). The overall, long term, 1σ, reproducibility of the method on silicate powders is given at 2‰ for δD.

Mineral abbreviations used in figures of this article follow recommendations by the IUGS Subcommission on the Systematics of Metamorphic Rocks: Web version 01.02.07 according to Kretz (1983) completed by Siivola and Schmid (2007).

4. Veins and dykes petrography and structure

4.1. Tremolite-antigorite veins

In addition to widespread lizardite mesh and lizardite-coated joints formed in relatively static conditions, which can be referred to “primary serpentinization” (see above), peridotites of the Peridotite Nappe are crosscut by tension and shear cracks filled with fibrous serpentine and amphibole. They appear independently of their location in the Peridotite Nappe and especially have no relation to the tectonic sole. Acicular/fibrous crack seals composed of antigorite (± chrysotile), tremolite, or both, are nucleated on lizardite seams (Fig. 3c, 3d, 4d, 5) and thus post-date them.

Fibrous amphiboles (anthophyllite and tremolite) are mainly present in Poro, Thio and Tiebaghi areas, but also appear in many other sites (Fig 1). In the Poro area (east coast) crack seals are filled with tremolite often associated with antigorite (Fig. 6), whereas in the Tiebaghi area vein infills are dominated by anthophyllite (Lahondère et al. 2012). In most cases, Raman analysis only allowed the determination of intimately intergrown tremolite and antigorite (Fig. 6 and 7). In the Massif du Sud crack infills comprised tremolite, anthophyllite and Mg-chlorite. Anthophyllite reaction rims generally appear at the margin of some felsic dykes and around peridotite enclaves within the same dykes. Crack seals with Mg-rich amphiboles appear closely related to felsic dykes in the Thio area (east coast). Microfaults with synkinematic fibrous tremolite and anthophyllite coatings crosscut dykes related to the lower Eocene dyke complex (Thio, Bogota Peninsula) (Lahondère and Maurizot 2009 ; Lahondère et al. 2011, 2012). Thus, field evidence and radiochronologic data from felsic dykes

suggest that amphibole-bearing veins, which are more or less associated with felsic magmatic dykes formed after 55 Ma.

Most synkinematic fibrous or acicular antigorite and tremolite crystals that appear in cm- to dm-thick open cracks and dikelets are:

- either strongly oblique or perpendicular to fissure walls and thus resemble tension cracks (Fig. 3c)
- or, slightly oblique to fissure walls and very much resemble to pull-apart crack seals associated with micro-faulting (oblique slip) (Fig. 3d)

These well-known tectonic features of brittle and semi-brittle rocks, which are extensively used for structural analysis, are generally filled with quartz, calcite and other minerals, depending on the composition of host rock (quartzite, limestone, etc.), which dominantly come from pressure/shear solution. Therefore, analogous process is postulated in serpentinized peridotites in which serpentine minerals are formed at medium to low temperature in the presence of water. In any case, these open tension or shear cracks are dilatational features, which likely record low lithostatic, or alternatively, relatively high fluid pressure.

In many places, tensile and shear fractures are closely associated and their fibres are aligned in the same direction, which represents the direction of maximum finite stretch ("X" axis of the local strain ellipsoid). When the vein thickness is larger than 5-10 cm, tremolite fibres are frequently organised in radiate or sheaf-like aggregates (Fig. 3a), which likely record fracture opening faster than synkinematic crystal growth. In some occurrences, first phase synkinematic fibrous crystals are micro-folded or crenulated during a second tectonic phase with different kinematic axes. It is worth noting that in this case, the second tectonic event generated antigorite only. Tremolite also appears in poly-mineral associations with antigorite, Mg-chlorite and magnetite in heaps and reaction structures.

4.2. Lower Eocene dykes

Lower Eocene supra-subduction magmas intruded the pre-existing fracture network as shown by the zig-zag geometry of some dykes (Cluzel et al. 2006); therefore, a relationship with serpentinization may be suspected (e.g., Python et al. 2011). However, not all dykes display lizardite walls and some of a zigzag geometry, display serpentinized and unserpentinized walls, depending upon fracture orientation. The only (scarce) occurrences of reaction rims around Eocene dykes are composed of relatively coarse-grain anthophyllite or Mg-chlorite. Therefore, lizardite “black walls” formed before dyke intrusion and cannot be related to peridotite-magma interaction.

In a few locations (Poro, Kopeto) dm- to m-thick “dykes” are composed of whitish massive material dominated by tremolite. Samples from these localities display high Ti and Al contents (eg. sample POR1b, see below) and are probably deeply altered HFSE-depleted felsic dykes (Cluzel et al.

2012), which contain no zircons that could be dated. Remarkably, the two tremolite types, synkinematic and reaction-type coexist on these outcrops, a fact that suggests a genetic relationship.

4.3. Structural analysis of lower Eocene dykes and tremolite-antigorite veins

Crosscutting dykes are found at all levels of the ophiolite, except in gabbronorite cumulates, which are crosscut by IAT dolerites only. Strongly fragmented dykes are also present in the porphyroclastic serpentinite sole, whereas they are well preserved in the rest of the Peridotite Nappe. It is worth noting that in contrast with Late Oligocene granitoids (Cluzel et al. 2005; Paquette and Cluzel 2007) Eocene dykes never crosscut the parautochthonous or autochtonous basement of the ophiolite, a feature consistent with their pre-obduction character. Most dykes trend NW-SE (av. N140°E) and NNE-SSW (av. N30°E), and some sills intruded parallel to the peridotite foliation. Their orientations are roughly consistent with the main structural trends of the Peridotite Nappe and locally, sub-parallel to antigorite and tremolite-bearing veins, but they rarely coexist. Most ultramafic, mafic and felsic intrusive rocks are medium to coarse grained and locally display pegmatite texture; in contrast, dolerites are fine-grained and often display chilled margins. Thin medium-temperature reaction rims with anthophyllite, talc, and chlorite, develop around most coarse-grained felsic dykes. In contrast, chilled margins of the younger dolerite dykes unambiguously show that they were emplaced at lower host rock temperatures. Locally (Massif du Sud, Ouen Isl.), coarse-grained diorite and hornblendite dykes are severely deformed and display ductile strain features including high-temperature foliation marked by amphibole preferred orientation, boudinage and stretching, plagioclase-hornblende banding and locally isoclinal folding (Ouen Isl.), evolving internally toward lower-temperature mylonite and cataclastic mylonite. Shallow dipping stretching lineation and/or hornblende preferred orientation suggest strike-slip or oblique slip tectonics; i.e., sinistral-reverse motion along N150°E trending dykes (Soret et al. 2016). U-Pb dating of zircon gave magmatic ages at ~55-52 Ma (Cluzel et al. 2006) close to $^{40}Ar/^{39}Ar$ hornblende cooling ages at ~55 Ma (Soret et al. 2016). The occurrence of internal ductile textures suggests synkinematic intrusion in a transcurrent tectonic regime. This event is thus slightly younger than amphibolites of the metamorphic sole, which record subduction initiation at ca. 57-56 Ma (Cluzel et al. 2012; Soret et al. 2016). It is worth noting that IAT dolerite dykes, which occur at about the same level of the Peridotite Nappe never display such tectonic features and thus post-date this event at ca. 50 Ma (Cluzel et al. 2012; Cluzel and Jourdan unpubl. $^{40}Ar/^{39}Ar$ data). These data also suggest significant unroofing of the Peridotite Nappe during the 55-50 Ma interval.

Most dykes apparently escaped the mineral transformations that commonly affect the host peridotite and have well preserved magmatic mineralogy; however, some display secondary development of epidote, albite and green amphibole (Rodgers 1973a, 1973b; Rodgers and Bevan 1974; Maurizot and Lesimple 2012) depending upon local thermal anomalies and/or fluid-rock ratio.

Therefore, the elemental mobility associated with greenschist alteration is likely to have occurred during or soon after dyke emplacement.

The oblique arrangement of the kinematic axes deduced from antigorite and tremolite-antigorite shear veins (Iseppi 2018) is consistent with the development of the oblique subduction postulated on the basis of paleogeographic and tectonic evidence (Cluzel et al. 2001; Maurizot and Cluzel 2014). Meanwhile, the development of "extensional" strain (i.e. shallow dipping stretching axis) in the upper plate of the subduction/obduction system is consistent with stress orientation in the upper plate in shallow subduction settings (Chemenda et al. 2000; Espurt et al. 2008; Gutscher et al. 2000; McCaffrey et al. 2000; McNulty and Farber 2002). Overall, it is consistent with the tectonic features that may develop at subduction inception (Fig. 15).

At island scale, the fracture network of the Peridotite Nappe shows a N130°E dominant trend, associated with subordinate N090°E, N045°E and N000°E directions (Leguéré 1976; Moutte and Paris 1977) that control most geomorphological features. At outcrop scale and near the base of the nappe, peridotites are affected by dense and complex fracture sets, which are probably due to several superimposed tectonic events during obduction and exhumation to shallow depth. Brittle failure at low lithostatic pressure accounts for changing stress ellipsoids and complex joint patterns. In contrast, antigorite and tremolite-antigorite veins, which characteristically have several meters to several tens of meters spacing and have been filled at relatively high temperature, display consistent structural orientations and likely originated from the same tectonic events independently of obduction.

Tremolite and antigorite appear in tension cracks, strike-slip, normal or reverse faults related to the frictional reactivation of pre-existing fractures. Inversion of fracture data from the Massif du Sud yields a sub-horizontal stretching axis of the strain ellipsoid with a roughly N-S (± 20°) orientation. In contrast, in the klippes of the northwest coast (Koniambo and Tiebaghi), the stretching axis is oriented WNW-ESE (Iseppi 2018). In general, the shortening axis, although variably oriented, is steeply dipping. The strain ellipsoid denotes transtensional setting in the upper plate of the subduction consistent with inception of oblique subduction (Gurnis et al. 2004; Gutscher et al. 2000).

5. Analytical results

5.1. Whole-rock geochemistry

Sampling has been undertaken in several nickel open pit mines throughout New Caledonia and ten samples from the Poro mine (east coast) judged representative, have been selected for chemical analysis (Table 2). Seven of these samples had been identified in the field as tremolite and three as antigorite taken for comparison. It appeared thereafter that most samples were not pure mineral phases but actually a mix of tremolite and other minerals (talc-chlorite, antigorite). By comparison

405 with theorical tremolite, only two samples are close to the pure end-member with only a limited
406 amount of Fe/Mg substitution, which accounts for the pale green colour of some prismatic crystals.
407 In a general fashion, trace elements contents in serpentinized harzburgite and dunite are very
408 low; similarly, REE contents of most antigorite samples are extremely low and below the detection
409 limit of routine analysis. However, the tremolite-bearing samples have contents higher than
410 serpentines; specifically, REE could have been analysed with a good accuracy by ICP-MS analysis. The
411 specific behaviour of Eu is worth noting; REE patterns of tremolite-bearing veins display positive Eu
412 anomalies (Fig. 8), which contrast with the negative anomaly of most felsic dykes due to feldspar
413 fractionation.
414
415 **5.2. Mineral chemistry**
416 Microprobe analyses of syntectonic tremolite needles/fibres on polished thin sections show some
417 variability without clear connection with location or textural features. On the $Fe/(Mg+Fe^{2+})$ vs. total
418 Si binary diagram (Leake 1968, Leake et al. 1997; Hawthorne et al. 2012), the analysed amphiboles
419 (Table 3) dominantly plot in the domain of tremolite and alternatively in the tremolite-hornblende
420 domain (Fig. 9) with a strong negative correlation between Mg# and total Si. Chromium content also
421 displays a close negative correlation with Si content (Fig. 10a) and a positive correlation with X_{FeA} (Fig.
422 10b), which both are indicative of increasing T° of crystallization. High-Mg chlorites associated with
423 tremolite in some veins ($0.29 < Fe_{tot} < 0.34$; $9.67 < Mg < 9.92$) may be termed penninites according to
424 Hey's classification (Hey, 1954); they are referred herein to as Mg-chlorites.
425
426 **5.3. Strontium isotopes**
427 The $^{87}Sr/^{86}Sr$ ratio is a possible marker of the origin of Ca in tremolite because Ca and Sr display
428 similar geochemical behaviour. The very low Ca and Sr content of antigorites makes the analysis
429 difficult as Sr contents are often below the detection limit of routine analysis (0.1 ppm). Therefore,
430 more analyses have been performed on purified minerals to get more accurate data to build the Sr
431 vs. $^{87}Sr/^{86}Sr$ diagram. On the Sr and Ca vs. $^{87}Sr/^{86}Sr$ diagrams (Fig. 11; Table 4), tremolite-bearing veins
432 plot in a narrow array with a negative slope (Fig. 11). The $^{87}Sr/^{86}Sr$ ratios of almost pure tremolite
433 (CaO= 9-12 wt%; Sr= 4-9 ppm) are in the range of 0.7042-0.7045. In contrast, antigorites, which have
434 very low Ca (0.002 wt%-0.01 wt% CaO) and Sr contents (0.03 ppm-1.4 ppm) display a wider range of
435 highly radiogenic $^{87}Sr/^{86}Sr$ ratios (0.7062-0.7116) without clear correlation with Ca or Sr contents.
436
437 **5.4. Oxygen and hydrogen isotopes**
438 Tremolite and serpentine minerals likely were in isotopic equilibrium with circulating/pore water
439 during their crystallization; therefore, isotopic compositions of minerals reflect that of water
440 (Méheut et al. 2010). Fresh tremolite and antigorite were carefully selected by hand picking and

analysed for oxygen and hydrogen isotopes, compared to weathered specimens and data from Ni-rich and Ni-poor supergene silicates: "garnierite" (an informal mixture of Ni-rich serpentine, talc and smectite) of New Caledonia (Amisse et al. 2010); and deweylite (Wenner and Taylor 1974) (Table 5). Isotopic ratios were plotted on the δD vs. $\delta^{18}O$ diagram (Fig. 12). Fresh tremolites (av. $\delta^{18}O$ = 6.8‰; δD = -54.8‰) and antigorites (av. $\delta^{18}O$ = 6.4‰; δD =-46.0‰) from this study plot in a narrow field similar to that of "continental antigorites" of Wenner and Taylor (1974); in contrast, tremolite and antigorite from the weathering profile of the same sites, have lower δD (-60‰ to -110‰) at somewhat constant $\delta^{18}O$. Fresh tremolite and antigorite have higher $\delta^{18}O$ and lower δD than supergene silicates (Amisse et al. 2010).

Serpentinites of the tectonic sole characteristically display supergene isotopic signatures (Ulrich 2010), which may due to infiltration of meteoric waters during obduction (Quesnel et al. 2013, 2016) or alternatively, post-obduction (i.e. post-kinematic) rock-water interaction. In any case, field evidence shows that tremolite-bearing veins predate and have no genetic relationship to the brittle shearing and fracture development related to obduction. Therefore, fresh tremolite and antigorite veins have been most likely formed in endogenous conditions and did not interact with meteoric water.

6. Discussion

Tremolite- and antigorite-bearing veins from the Peridotite Nappe of New Caledonia display geochemical and isotopic features that drastically contrast with their host rocks. Prominent enrichment of tremolite-bearing veins in some major and trace elements compared to serpentinized peridotites, and the synkinematic character of fracture infill suggest that they likely formed at depth through a metasomatic process in connection with minor tectonic events. Their geochemical and isotopic composition thus results from the interaction of several potential solid and fluid sources, the role of which may vary through time. Solid sources are represented by the variably serpentinized peridotite host rocks and the lower Eocene dykes which crosscut them, while fluid sources may be the fluids that circulated in the supra-subduction mantle; i.e., mostly aqueous fluids released by slab dehydration.

6.1. Textural features, relative chronology and temperature constraints

Much attention has been paid to ultramafic terranes having undergone HP-LT metamorphism in subduction/collision zones. For example, the stability fields of serpentine minerals have been mainly defined at high pressure (e.g., Debret et al. 2013; Deschamps et al. 2013; Schwartz et al. 2013; Padrón-Navarta et al. 2010, 2013). In contrast, data from low-pressure ultramafic terranes are scarce, except those retrieved by ocean drilling programs, which generally correspond to serpentinite bodies exhumed at magma-poor extensional systems or at transform faults. The Peridotite Nappe of

New Caledonia is a supra-subduction ophiolite (see geological setting above and Fig. 15) and although there are no precise P-T constraints available, its evolution lacked high pressure conditions and is probably similar to “oceanic” terranes at least during the first steps.

Syntectonic antigorite and tremolite-antigorite bearing veins crosscut and frequently reactivate (re-open) lizardite veins formed during “primary” pervasive serpentinization. Instead of static pseudomorphic replacement of the high-temperature parageneses (olivine + Opx) by relatively low-temperature lizardite and brucite, they record shearing deformation due to a low-strain tectonic event. Some tremolite-bearing veins display final crystallization of antigorite. Thus, a rough chronology may be established as follows: 1) early tremolite (mostly erased); 2) static lizardite (± chrysotile); 3) synkinematic antigorite or antigorite + tremolite, 4) synkinematic antigorite solely, 5) supergene minerals.

In spite of some uncertainty on boundaries, this mineral sequence allows some constraints on the evolution in temperature to be proposed. The upper stability limit of lizardite (± chrysotile) at low pressure (< 0.4 GPa) is established to about 300-320°C (Evans, 2004), while antigorite stability starts at about 320°C and persists up to 500-550°C (Wenner and Taylor, 1971). At low to medium pressure (0.1-0.5 GPa) tremolite appears at 350-550°C and disappears at 400-650°C depending on the CO_2 partial pressure (Jenkins 1983; Chernosky et al. 1998; Evans 2004; Evans et al. 2000, 2013). Therefore, the relative chronology above records: 1) a net increase in temperature after primary serpentinization, during the formation of tremolite-antigorite-bearing veins; 2) a gentle temperature decrease at the end of tremolite crystallization; and 3) a final temperature decrease down to supergene conditions (ca. 50-35°C).

The total thickness of the Peridotite Nappe does not exceed 2 km; therefore, a depth-dependent variation of temperature is unlikely and with the exception of chrysotile, which seems to be more concentrated near the tectonic sole, there is no specific location for tremolite- or antigorite-bearing veins.

6.2. Selective input of incompatible trace-elements record of tremolite-bearing veins

Tremolite-bearing veins are generally enriched by about 10 to 100 times in REE and incompatible elements compared to peridotite host rock and commonly display positive Eu (Fig. 8) and negative Zr-Hf anomalies (Fig. 13).

Positive Eu anomalies have been described in peridotite-hosted hydrothermal fluids (Allen and Seyfrid 2003, 2005; Schmidt et al. 2007) and in serpentines of mid-oceanic ridges (German et al. 1999; Douville et al. 2002; Paulick et al. 2006, Ningthoujam et al. 2012) and thus, early hydrothermal circulations could be a source for REE. However, Eu anomalies do not appear in serpentinized dunites and harzburgites of the Peridotite Nappe and only secondarily silicified and carbonated rocks of the serpentinite sole display bulk REE enrichment (~10 times) especially in LREE (Ulrich 2010; Fig.

7). Rare Earths Elements patterns of moderately silicified and carbonated serpentines characteristically display Ce negative anomalies. This feature is diagnostic of REE enrichment of supergene origin because Ce^{4+} is residual during oxidizing alteration and accumulates with hematite on top of the weathering profile (Braun et al. 1990); therefore, supergene fluids circulating from the weathering profile were probably Ce-depleted. Thus, high REE content of tremolite-bearing veins is likely unrelated to supergene alteration and of probable hydrothermal origin, the hydrothermal fluids having interacted with feldspar in order to acquire a positive Eu anomaly. Owing to the relative chronology established above, REE enrichment most likely appeared after primary serpentinization, during subsequent water-wall rock interaction.

Although tremolite-bearing veins have obviously not been generated by magmatic processes, the contrasting behaviour of Eu compared to other REE is possibly a key for REE provenance. The REE patterns of tremolite-bearing veins analysed in this study, display a positive Eu anomaly, which has the same order of magnitude regardless of the bulk REE content. Eu anomalies in tremolite-bearing veins may have been caused by precipitation of tremolite from solutions which had already developed Eu anomalies. Therefore, a positive Eu anomaly in tremolite may possibly come from reaction with fluids having altered a plagioclase-rich rock such as a gabbro cumulate or a felsic dyke.

Assessing the enrichment of tremolite veins in some trace-elements compared to peridotites/serpentinites is not always possible because some trace-element abundances in the latter are below the standard detection limit (Secchiari et al. 2019; table 2). When measurable, this enrichment is not uniform and prominent depletion appears in HFSE (Nb, Ta, Zr and Hf), some of which are below the detection limit of standard ICPMS whole rock analysis (Table 2). HFSE depletion is a common feature of subduction zone magmatism, and generally interpreted to result from the occurrence of HFSE-retaining residual minerals in the subducting slab (e.g. Garrido et al. 2005; Holm et al. 2016; Munker et al. 2004 ; Rubatto et al. 2003; Woodhead et al. 2011); consequently, HFSE-depleted fluids are transferred toward the mantle wedge. Therefore, fluids directly emitted by the subduction could have circulated in the supra-subduction mantle (Fig. 14b) and generated tremolite-antigorite veins with a similarly HFSE-depleted signature. However, strontium, oxygen and hydrogen isotopic features of tremolite are not consistent with direct slab derivation and point to a "magmatic" signature (see 6.4 and 6.6 below).

In contrast to most subduction zone magmatic rocks, Eocene supra-subduction dykes of the Peridotite Nappe dominantly display strong positive Zr and Hf anomalies (~10 times) and contain abundant magmatic zircons (Cluzel et al. 2006). Hydrothermal fluids circulating in fractures hosting Eocene dykes may be relatively depleted in certain elements contained in refractory minerals and this is possibly the case for Hf and Zr captured by zircon and other Hf- and Zr-retaining minerals. At moderate temperature within the tremolite stability domain (<600°C), Ca and other mobile elements may have been leached from dykes, while magmatic zircons remained unaffected, thus resulting in

549 Zr-Hf depletion in circulating fluids. In contrast, leaching of peridotites or felsic cumulates
550 (gabbronorites), which do not contain zircon would not result in such a feature and thus can be
551 discarded. Preferential Ca leaching may also be expected by autometamorphism of some dykes. By
552 the end of crystallization, supercritical hydrous fluids originally contained in the magma (2% to 10%
553 depending upon magma composition) are ejected at sub-solidus temperatures. This process was
554 likely responsible for the appearance of secondary amphibolite to greenschist facies parageneses in
555 some dykes and favoured the development of ductile tectonic features (banding, preferred
556 orientation, isoclinal folding, mylonitization) within some dykes, which did not appear in the
557 peridotite host
558
559 **6.3. Origin of antigorite veins, constraints from Sr isotopes.**
560 The $^{87}Sr/^{86}Sr$ ratio in harzburgites and lherzolites of the Peridotite Nappe, which are the most
561 common wall rocks of antigorite and tremolite-bearing veins, covers a relatively large range (0.7049-
562 0.7077) (Secchiari 2016; Secchiari et al. 2019) and a certain role of "primary" serpentinization may be
563 suspected. However, there is no correlation between the LOI, which could represent the degree of
564 primary serpentinization and Sr isotope ratio of unserpentinized (LOI= 0%-0.7%; $(^{87}Sr/^{86}Sr)_i$= 0.7077-
565 0.7054) and moderately serpentinized lherzolites and harzburgites (LOI= 6.0%-10.7%; $(^{87}Sr/^{86}Sr)_i$ =
566 0.7075-0.7049) (Seccchiari et al. 2016; 2019). Thus, a moderate amount of primary serpentinization
567 does not significantly change the Sr isotope ratio of peridotites. Therefore, serpentinization cannot
568 be directly responsible for the radiogenic character and variability of the $^{87}Sr/^{86}Sr$ ratio of New
569 Caledonia's peridotites, which are thus likely due to slab-derived magma input (Secchiari et al. 2019).
570 As far as shear- or pressure-solution origin is considered for antigorite veins, the Sr isotope
571 composition of antigorite is expected to reflect the variability of peridotite wall rock, pending some
572 influence of circulating fluids. However, the $^{87}Sr/^{86}Sr$ of antigorite veins is much higher than that of
573 peridotites (up to 0.7117), close to the present ocean water composition and even much higher than
574 that of lower Eocene waters (Murthy and Beiser 1968; Elderfield 1986; Veizer 1989; McArthur et al.
575 2012). These values are slightly lower than that of hemi-pelagic terrigenous sediments (e.g.
576 McLennan et al. 1990; Hemming et al. 2007) and infer sediment-water mixing/leaching. Thus, the
577 highly radiogenic $^{87}Sr/^{86}Sr$ ratios from antigorite veins (Fig. 11) may reflect some influence of
578 subducted sediments on the fluids emitted by the subduction zone, which infiltrated the supra-
579 subduction mantle and were involved in antigorite crystallization. The nature of involved sediments
580 remains unknown; however, Late Cretaceous sediments similar to those included in the Poya
581 Terrane; abyssal argillites associated with basalts and hemipelagic turbidites of the Kone Facies, are
582 good candidates for the source of high $^{87}Sr/^{86}Sr$ fluids. At that stage, there are no constraints on the
583 mechanisms and P-T conditions of fluid release from the slab.
584

585 **6.4. Origin of Ca in tremolite-bearing veins, constraints from Sr isotopes.**

586 Tremolites from veins and pockets plot in a narrow field with low $^{87}Sr/^{86}Sr$ (0.7042-0.7045), that
587 clearly differ from the isotopic signatures of lherzolites and harzburgites; thus, a direct origin of Ca by
588 leaching of peridotites is unlikely. Alternatively, tremolite seems to have been in equilibrium with
589 "magmatic" fluids (Fig. 11); a feature consistent with $\delta^{18}O$ and δH values (see below), even though a
590 certain influence of ocean-like water cannot be excluded. The "sedimentary" signature of antigorite
591 veins, possibly derived from subduction-related fluids (see 6.3 above), was probably diluted in
592 tremolite-bearing veins, which contain 100 to 1000 times more Sr than antigorite.

593 A comparison with exhumed serpentinites of the Atlantis Massif (Boschi et al. 2008) shows that
594 similar trends may exist in oceanic ridge environments; variable Ca-Sr contents at high and constant
595 $^{87}Sr/^{86}Sr$ ratio record metasomatism from oceanic water/sediments, while additional Ca-Sr
596 enrichment with decreasing $^{87}Sr/^{86}Sr$ signals some influence of (crustal ?) magmatic rocks (Fig. 11).

597 It is unlikely that tremolite formed by direct reaction of felsic magma with serpentinized wall rock,
598 because in all observed reaction rims around dykes, anthophyllite and/or Mg-chlorite are formed
599 instead of tremolite. In the frequent absence of direct contact between felsic dykes and tremolite
600 veins or pockets, it may be suggested that tremolite merely formed by reaction between hydrous
601 fluids released by the subduction zone and having leached the still hot felsic dykes and the
602 serpentinized wall rocks of active shears or tension cracks. This may account for the compositional
603 variability, REE contents 10 times lower than that of dykes and the presence of large amounts of
604 compatible elements taken from fracture walls. Thus, three end-members are likely involved in the
605 formation of tremolite: 1) an aqueous fluid emitted from the subduction zone and somewhat
606 influenced by sediments; 2) a REE-poor and compatible elements-rich ultramafic end-member that
607 displays variable Sr isotope signature; and 3) a REE-rich magmatic end-member with a mantle-like
608 isotopic signature, which very much resembles Lower Eocene dykes, or fluids evolved from these
609 dykes.

610

611 **6.5. High Cr contents and wall rock involvement**

612 An important geochemical feature of New Caledonia tremolites is the high content of compatible
613 trace elements such as Cr (Fig. 9). Cr is relatively immobile in hydrothermal and supergene systems
614 and should appear in tremolite with moderate contents only. Whole-rock analysis of tremolite-
615 bearing veins revealed high Cr contents (2,800 – 3,300 ppm), which may be due to Cr contained in
616 newly crystallized (syn-kinematic) minerals, or alternatively, to residual chromite. However,
617 microprobe analyses of tremolites display up to 2.6 wt% Cr_2O_3 (Table 3). Cr content correlates
618 negatively with total Si (Fig. 10a) and positively with Fe content (XFeA = 100(Fe+Mn)/(Fe+Mn+Mg)
619 (Fig. 10b), a feature that suggests increasing Cr incorporation with higher temperature. The
620 polymineralic tremolite-bearing veins and pockets coming from the replacement of peridotite along

fractures contain residual streaks of chromite, which display evidence for Cr mobility. Altered chromites are generally composed of a residual chromite core rimmed by a microcrystalline association of chromite and Cr-rich magnetite (Fig. 13). Fe-Cr substitution giving birth to Cr-rich magnetite may be responsible for Cr mobility and its incorporation into tremolite. Therefore, high Cr contents in tremolite may be explained by an intervening Cr-rich end-member during water rock interaction, which is most likely the peridotite wall rock.

The mobility of Cr in hydrous fluids strongly depends on its oxidation state; whereas Cr^{3+} species are relatively immobile, Cr^{6+} are highly mobile (e.g. James, 2003). Thus chromite dissolution and formation of Cr-rich magnetite rims around inherited chromite grains needs oxidizing fluids consistent with the preferential leaching of Eu from felsic dykes and occurrence of positive Eu anomalies in tremolite. Oxidized character is a feature of fluids emitted by subduction zones that involve highly serpentinized upper mantle rocks (Evans et al. 2017). Nothing is known about the degree of primary serpentinization of the lower plate of the subduction/obduction system of New Caledonia, which has totally disappeared in the subduction zone, whereas its partial preservation in the exhumed eclogitic melange (Pouebo Terrane) is problematical. However, considering that the degree of serpentinization of the upper and lower plates might have been identical prior to subduction inception, it may be postulated that an important part of the serpentinization of the Peridotite Nappe was acquired prior to subduction and is unrelated to obduction.

6.6. Origin of the tremolite- and antigorite-precipitating fluids

The $\delta^{18}O$ and δD of hydrous minerals result from complex balance of several parameters: the isotopic composition of the wall rock, the water/rock ratio, mineral-water fractionation coefficients, isotope ratios of circulating water, and temperature. In this study, a probable temperature of tremolite-antigorite formation can be estimated in the range 300-450°C (end of section 6.2). Under these temperatures, tremolite and serpentine minerals should display comparable $\delta^{18}O$ values as an equilibrium isotopic fractionation of about $\delta^{18}O_{Trem\text{-}Serp}$ = -0.3‰ is expected (Zheng, 1993). The mean $\delta^{18}O$ values depicted above (6.8‰ and 6.4‰ for tremolite and antigorite, respectively, corresponding to $\delta^{18}O_{Trem\text{-}Serp}$ = +0.4‰) are somewhat at variance with the theoretical equilibrium. In fact, in the crystallizing sequence (end of section 6.2), we argue for a slight temperature decrease at the end of tremolite crystallization. All other things equal, this should imply a small increase of the isotopic fractionation between tremolite and water, and thus an increase in the $\delta^{18}O$ value of tremolite. The fact that tremolite is actually slightly enriched ($\delta^{18}O$ = 6.8‰) in ^{18}O relative to antigorite ($\delta^{18}O$ = 6.4‰) is consistent with a small temperature decrease.

It remains that, at first order, both minerals likely crystallized in equilibrium with a unique aqueous reservoir. Assuming then that fluid was in excess at the time of vein formation (i. e., the fluid/rock ratio is isotopically infinite, which was very likely in the case of the studied veins), the $\delta^{18}O$

value of the invading fluid can be estimated between 6.5‰ and 8.5‰ (using the fractionation factors between H_2O and serpentine and antigorite between 300 and 450°C from Zheng, 1993). These values are consistently expected for the fluids involved in supra-subduction contexts, like the one prevailing for the formation of the studied veins. Indeed, these fluids, originally derived from seawater, underwent significant isotopic exchange with crustal and mantle rocks, as shown by the Sr isotope and REE systematics of vein minerals, which results in increasing their initial, low $\delta^{18}O$ value. A magmatic contribution to the fluid budget that would add a high- $\delta^{18}O$ component (about 7‰) to the fluid is permitted by the data.

From the observations presented above, it appears that lizardite formed during the primary serpentinization did not significantly recrystallize when the rock went into the antigorite stability field. It should be kept in mind that lizardite and antigorite may coexist at low pressure depending upon serpentine composition (e.g., Caruso and Chernosky 1979; O'Hanley et al. 1989; Schwartz et al. 2013). However, antigorite fibres in the study are nucleated on lizardite "black walls" and partly originated from the destabilization of lizardite as shown by the accumulation of iron oxide at the lizardite-antigorite interface (Fig. 4c & 4d). However, the pervasive replacement of "primary" lizardite by antigorite would require an unlikely large water/rock ratio given the relative impermeability of lizardite coatings and restriction of fluid circulation along open fractures.

It is worth noting that some serpentine samples from open pit mines did not escape tropical weathering and yield strongly negative δD ratios similar to that of supergene silicates. In order to evaluate the effect of weathering, four samples of the same steep antigorite vein were taken across the weathering profile of Vulcain mine. Upward decreasing δD values (-38.7‰ > δD > -107.2‰; Table 5) unambiguously show that only unweathered antigorites taken in the bedrock retain their original isotopic signature. In addition, rocks of the serpentinite sole display strongly negative δD (-80‰<δD<-105‰) (Fig. 12; Ulrich 2012); thus, these otherwise unweathered rocks have been profoundly modified by fluids of supergene origin as also shown by their negative Ce anomaly.

7. Conclusion

The formation of tremolite- and antigorite-bearing veins recorded an elevation of temperature compared to the initial oceanic (primary) serpentinization of peridotites, which was marked by the formation of lizardite and minor chrysotile; therefore, a heat source is needed as well as a source for Ca. This event was associated with shear/tensile reactivation of pre-existing joints already coated by lizardite.

The widespread antigorite-bearing low-Ca veins bear highly radiogenic $^{87}Sr/^{86}Sr$ signatures, which record some influence of subducted sediments. In contrast, this "sedimentary" signature is diluted in high-Ca tremolite, which probably comes from Ca input of direct or indirect magmatic origin. The Sr isotope signature of tremolite, the REE abundance, the $\delta^{18}O$ and δD values, all suggest that the Ca

source was the supra-subduction Early Eocene felsic dyke system and thus indirectly, the subducted slab. Europium positive anomaly and paradoxically high contents of some compatible elements (Cr) suggests that Ca was carried by oxidized hydrothermal fluids that leached the dykes and interacted with Cr-rich wall rock (serpentinized peridotite). These features provide a constraint on the timing of tremolite crystallization, because supra-subduction dykes intruded peridotites within a narrow span of time at ca. 55-50 Ma (U-Pb zircon; Cluzel et al. 2006). Since these dykes are mostly slab melts and boninite-series magmas that formed shortly after subduction inception (Cluzel et al. 2012, 2016), already existing fractures were reactivated in an oblique-extensional regime under relatively high fluid pressure and gave way to magma and laterally/upward to Ca-bearing fluids when the young and buoyant slab had to force its way beneath the nascent fore-arc lithosphere (Fig. 14). The heat source needed for crystallizing tremolite and antigorite after lizardite was likely provided by the injection of supra-subduction slab melts. The coexistence of tremolite and antigorite in the same fracture fillings, and thereafter crystallization of antigorite solely, could signal the exhaustion of magmatic fluids, while synkinematic crystallization associated with small-scale fault motion and tension cracks was continuing. It also signals that tremolite and antigorite veins were related to the same tectonic event, whereas only fluid composition differed through time.

Therefore, independent of decreasing-upward serpentinization due to the obduction of the Peridotite Nappe, the development of tremolite-antigorite veins may be related to a three-step evolution: i) the “oceanic” period (Late Cretaceous-Paleocene), during which static serpentinization developed along cooling joints (Fig. 14a); ii) at subduction inception (latest Paleocene), when the injection of slab-derived supra-subduction magmas and fluids, together with semi-brittle shearing due to tectonic deformation of the upper plate of the system generated the tremolite-antigorite vein system (Fig. 14b); finally, iii) the fluid-assisted melting of the supra-subduction mantle generated strongly depleted melts, the fractionation of which resulted in gabbronorite cumulates (Fig. 14c) that now represent the only remnants of fore-arc crust.

Acknowledgements

This study is a contribution of CNRT Nickel et son Environnement research programs « Amiante-serpentinisation et fibrogenèse dans les massifs de péridotite de Nouvelle-Calédonie » and « Ophiostruct-Connaissance de l’ophiolite, structure et géophysique aéroportée ». T. Rigaudier (CRPG, Vandœuvre-lès-Nancy, France) is warmly thanked for assistance in isotope analyses. We acknowledge Professor Katy Evans and an anonymous reviewer for their constructive reviews.

References

Adams CJ, Beck RJ and Campbell HJ (2007) Characterisation and origin of New Zealand nephrite jade using its strontium isotopic signature. Lithos 97: 307-322. https://doi.org/10.1016/j.lithos.2007.01.001

Adams CJ, and Beck RJ (2009) A signature for nephrite jade using its strontium isotopic composition: some Pacific Rim examples. Journal of Gemmology 31: 153-152.

Agrinier P, Cornen G, Beslier M-O (1996). Mineralogical and oxygen isotopic features of serpentinites recovered from the ocean/continent transition in the Iberia abyssal plain. In: Whitmarsh RB, Sawyer DS, Klaus A, and Masson DG (Eds.), Proceedings of the Ocean Drilling Program, Scientific Results 149: 541-549.

Agrinier P and Cannat M (1997) Oxygen-isotope constraints on serpentinization processes in ultramafic rocks from the Mid-Atlantic Ridge (23° N). In: Karson, J.A., Cannat M,Miller DJ, and Elthon D (Eds.). Proceedings of the Ocean Drilling Program, Scientific Results 153: 381-388.

Allen D and Seyfrid WE Jr (2003) Compositional controls on vent fluids from ultramafic-hosted hydrothermal systems at mid-ocean ridges: An experimental study at 400°C, 500 bars. Geochimica et Cosmochimica Acta 67: 1531-1542 https://doi.org/10.1016/S0016-7037(02)01173-0

Allen DE and Seyfrid WE Jr (2005) REE controls in ultramafic hosted MOR hydrothermal systems: An experimental study at elevated temperature and pressure. Geochimica et Cosmochimica Acta 69:675-683. https://doi.org/10.1016/j.gca.2004.07.016

Amisse L, Bergé J, Boulvais Ph, Cathelineau M, Dublet G, Fritsch E, Cluzel D, Mösser-Ruck R, Fandeur D and Juillot F (2010) Composition isotopique en O et H des veines de garniérite de Nouvelle-Calédonie. 23ème RST Bordeaux 25-29 octobre 2010.

Andreani M, Mével C, Boullier A-M, and Escartín J (2007) Dynamic control on serpentine crystallization in veins: Constraints on hydration processes in oceanic peridotites, Geochemistry Geophysics Geosystems 8: Q02012 https://doi.org/10.1029/2006GC001373

Avias J (1967) Overthrust structure of the main ultrabasic New Caledonian massives. Tectonophysics 4: 531-541 https://doi.org/10.1016/0040-1951(67)90017-0

Bach W and Klein F (2009) The petrology of seafloor rodingites: Insights from geochemical reaction path modelling Lithos 112: 103–117 https://doi.org/10.1016/j.lithos.2008.10.022

Baghat SS and Marshak S (1990) Microlithon alteration associated with development of solution cleavage in argillaceous limestone: textural, trace-elemental and stable-isotopic observations Journal of Structural Geology 12: 165-175 https://doi.org/10.1016/0191-8141(90)90002-G

Beach A (1974) A geochemical investigation of pressure solution and the formation of veins in a deformed greywacke. Contributions to Mineralogy and Petrology 46: 61–68 https://doi.org/10.1007/BF00377993

763 Beach A (1977) Vein arrays, hydraulic fractures and pressure-solution structures in a deformed
764 flysch sequence S.W. England. Tectonophysics 40: 201-225 https://doi.org/10.1016/0040-
765 1951(77)90066-X
766 Bell DR and Ihinger PhD (2000) The isotopic composition of hydrogen in nominally anhydrous
767 mantle minerals. Geochimica et Cosmochimica Acta 64: 2109–2118 https://doi.org/10.1016/S0016-
768 7037(99)00440-8
769 Bigeleisen J, Perlman ML and Posser HC (1952) Conversion of hydrogenic materials to hydrogen
770 for isotopic analyses Analytical Chemistry 24: 1356–1357 https://doi.org/10.1021/ac60068a025
771 Bons P and Jessell M (1997) Experimental simulation of the formation of fibrous veins by
772 localised dissolution–precipitation creep Mineralogical Magazine 61: 53–63
773 Boschi C, Dini A, Früh-Green GL and Kelley DS (2008) Isotopic and element exchange during
774 serpentinization and metasomatism at the Atlantis Massif (MAR 30°N): Insights from B and Sr isotope
775 data. Geochimica et Cosmochimica Acta 72: 1801-1823 https://doi,org/10,1016/j,gca,2008,01,013
776 Braun JJ, Pagel M, Muller JP, Billong P, Michard A and Guillet B (1990) Cerium anomalies in
777 lateritic profiles. Geochimica et Cosmochimica Acta 54: 781-795 https://doi.org/10.1016/0016-
778 7037(90)90373-S
779 Butt CW and Cluzel D (2013) Laterite Nickel ore deposits: weatherered serpentinites. Special
780 Issue “serpentines” Elements 9: 123-128 https://doi.org/10.2113/gselements.9.2.123
781 Caruso LJ and Chernosky JV Jr. (1979) The stability of lizardite. Canadian Mineralogist 17: 757-
782 769.
783 Chemenda A, Lallemand S and Bokun A (2000) Strain partitioning and interplate friction in
784 oblique subduction zones: Constraints provided by experimental modelling. Journal of Geophysical
785 Research 105: 5567–5581 https://doi.org/10.1029/1999JB900332
786 Chernosky JV, Berman RG and Jenkins DM (1998) The stability of tremolite: new experimental
787 data and a thermodynamic assessment. American Mineralogist 83: 726-739
788 https://doi.org/10.2138/am-1998-7-805
789 Clayton RN and Mayeda TK (1963) The use of bromine pentafluoride in the extraction of oxygen
790 from oxides and silicates for isotopic analysis. Geochimica et Cosmochimica Acta 27: 43-52
791 https://doi.org/10.1016/0016-7037(63)90071-1
792 Cluzel D, Bosch D, Paquette JL, Lemennicier Y, Montjoie Ph and Ménot RP (2005) Late Oligocene
793 post-obduction granitoids of New Caledonia: a case for reactivated subduction and slab break-off.
794 The Island Arc 14: 254-271 https://doi.org/10.1111/j.1440-1738.2005.00470.x
795 Cluzel D, Meffre S, Maurizot P and Crawford AJ (2006) Earliest Eocene (53 Ma) convergence in
796 the Southwest Pacific; evidence from pre-obduction dikes in the ophiolite of New Caledonia. Terra
797 Nova 18: 395-402 https://doi.org/10.1111/j.1365-3121.2006.00704.x

798 Cluzel D, Jourdan F, Meffre S, Maurizot P and Lesimple S (2012) The metamorphic sole of New
799 Caledonia ophiolite; $^{40}Ar/^{39}Ar$, U-Pb, and geochemical evidence for subduction inception at a
800 spreading ridge. Tectonics 31, 3 https://doi.org/10.1029/2011TC003085
801 Cluzel D, Ulrich M, Jourdan F, Paquette JL, Audet MA, Secchiari A and Maurizot P (2016) Early
802 Eocene clinoenstatite boninite and boninite-series dikes of the ophiolite of New Caledonia; a witness
803 of slab-melt enrichment of the mantle wedge in a nascent volcanic arc. Lithos 260: 429-442
804 https://doi.org/10.1016/j.lithos.2016.04.031
805 Cluzel D, Whitten M, Meffre S, Aitchison JC and Maurizot P (2017) A reappraisal of the Poya
806 Terrane (New Caledonia). Accreted Late Cretaceous marginal basin upper crust, passive margin
807 sediments and Eocene E-MORB sill complex. Tectonics 37: 48-70
808 https://doi.org/10.1002/2017TC004579
809 Collot JY, Malahof A, Recy J, Latham G and Missegue F (1987) Overthrust emplacement of New
810 Caledonia ophiolite: geophysical evidence. Tectonics 6: 215-232
811 https://doi.org/10.1029/TC006i003p00215
812 Craig H (1961) Isotopic variations in meteoric waters. Science 133: 1702-1703
813 https://doi.org/10.1126/science.133.3465.1702
814 Debret B, Andreani M, Godard M, Nicollet C, Schwartz S and Lafay R (2013) Trace element
815 behavior during serpentinization/de-serpentinization of an eclogitized oceanic lithosphere: A LA-
816 ICPMS study of the Lanzo ultramafic massif (Western Alps). Chemical Geology 357: 117-133
817 https://doi.org/10.1016/j.chemgeo.2013.08.025
818 Deschamps F, Godard M, Guillot S and Hattori K (2013) Geochemistry of subduction zone
819 serpentinites: A review. Lithos 178: 96–127. http://dx.doi.org/10.1016/j.lithos.2013.05.019
820 Dorling M and Zussman J (1987) Characteristics of asbestiform and non-asbestiform calcic
821 amphiboles. Lithos 20: 469-489 https://doi.org/10.1016/0024-4937(87)90030-2
822 Douville E, Charlou JL, Oelkers EH, Bienvenu P, Jove Colon CF, Donval JP, Fouquet Y, Prieur D and
823 Appriou P (2002) The rainbow vent fluids (26°14'N, MAR): the influence of ultramafic rocks and
824 phase separation on trace metal content in Mid-Atlantic Ridge hydrothermal fluids. Chemical
825 Geology 184: 37–48 https://doi.org/10.1016/S0009-2541(01)00351-5
826 Durney DW (1972) Solution-transfer, an important geological deformation mechanism. Nature
827 235: 315-317 https://doi.org/10.1038/235315a0DO
828 Durney DW (1976) Pressure-solution and crystallization deformation. Philosophical Transactions
829 of the Royal Society of London. Series A, Mathematical and Physical Sciences 283, 1312, A Discussion
830 on Natural Strain and Geological Structure, 229-240.
831 Elderfield H (1986) Strontium isotope stratigraphy. Palaeogeography, Palaeoclimatology,
832 Palaeoecology 57: 71-90 https://doi.org/10.1016/0031-0182(86)90007-6

833 Espurt N, Funiciello F, Martinod J, Guillaume B, Regard V, Faccenna C and Brusset S (2008) Flat
834 subduction dynamics and deformation of the South American plate: Insights from analog modeling.
835 Tectonics 27: TC3011 https://doi.org/10 .1029 /2007TC002175
836 Evans BW (2004) The serpentinite multisystem revisited: chrysotile is metastable, International
837 Geology Review 46: 479-506 http://dx.doi.org/10.2747/0020-6814.46.6.479
838 Evans BW, Ghiorso MS and Kuehner SM (2000) Thermodynamic properties of tremolite: A
839 correction and some comments. American Mineralogist 85: 466-472 https://doi.org/10.2138/am-
840 2000-0407
841 Evans BW, Hattori K and Baronnet A (2013) Serpentinite: What, Why, Where? Elements 9:99-106
842 https://doi.org/10.2113/gselements.9.2.99
843 Evans KA, Reddy SM, Tomkins AG, Crossley RJ and Frost BR (2017) Effects of geodynamic setting
844 on the redox state of fluids released by subducted mantle lithosphere. Lithos 278: 26-42.
845 https://doi.org/10.1016/j.lithos.2016.12.023
846 Evensen NM, Hamilton P J and O'Nions RK (1978) Rare earth abundance in chondritic meteorites.
847 Geochimica et Cosmochimica Acta 42: 1199–212 https://doi.org/10.1016/0016-7037(78)90114-X
848 Frost BR, Evans KA, Swapp SM, Beard JS and Mothersole FE (2013) The process of
849 serpentinization in dunite from New Caledonia. Lithos 178: 24-39
850 http://dx.doi.org/10.1016/j.lithos.2013.02.002
851 German CR, Hergt J, Palmer MR and Edmond JM (1999) Geochemistry of a hydrothermal
852 sediment core from the OBS vent-field, 21° N East Pacific Rise. Chemical Geology 155: 65-75
853 https://doi.org/10.1016/S0009-2541(98)00141-7
854 Gurnis M, Hall C and Lavier L (2006) Evolving force balance during incipient subduction.
855 Geochemistry Geophysics Geosystems 5, 7 https://doi.org/10.1029/2003GC000681
856 Gutscher MA, Spakman W, Bijwaard H and Engdahl ER (2000) Geodynamics of flat subduction:
857 Seismicity and tomographic constraints from the Andean margin. Tectonics 19: 814–833
858 https://doi.org/10 .1029 /1999TC001152
859 Hawthorne FC, Oberti R, Harlow GE, Maresch WV, Martin RF, Schumacher JC and Welch MD
860 (2012) Nomenclature of the amphibole supergroup. American Mineralogist 97: 2031–2048
861 http://dx.doi.org/10.2138/am.2012.4276
862 Harlow GE and Sorensen SS (2005) Jade (Nephrite and Jadeitite) and Serpentinite: Metasomatic
863 Connections. International Geology Review 47: 113-146 https://doi.org/10.2747/0020-6814.47.2.113
864 Hemming SR, Van de Flierdt T, Goldstein SL, Franzese AM, Roy M, Gastineau G and Landrot G
865 (2007) Strontium isotope tracing of terrigenous sediment dispersal in the Antarctic Circumpolar
866 Current: Implications for constraining frontal positions. Geochemistry, Geophysics, Geosystems, 8 (6)
867 http://doi.org/10.1029/2006GC001441
868 Hey MH (1954) A new review of the chlorites. Mineralogical Magazine 30: 277-92

Holm PM, Søager N, Alfastsen M and Bertotto GW (2016) Subduction zone mantle enrichment by fluids and Zr–Hf-depleted crustal melts as indicated by backarc basalts of the Southern Volcanic Zone, Argentina. Lithos 262: 135–152 http://dx.doi.org/10.1016/j.lithos.2016.06.029

Iseppi M (2018) Polyphase brittle tectonics and structural controls of supergene nickel ore deposits of New Caledonia. New exploration methods and ore deposit models. PhD Thesis University of New Caledonia, Noumea New Caledonia.

Jenkins DM (1983) Stability and composition relations of calcic amphiboles in ultramafic rocks. Contributions to Mineralogy and Petrology 83: 375-384 https://doi.org/10.1007/BF00371206

Kodolányi J, Pettke T, Spandler C, Kamber BS and Gméling K (2012) Geochemistry of ocean floor and fore-arc serpentinites: constraints on the ultramafic input to subduction zones. Journal of Petrology 53: 235-270 https://doi.org/10.1093/petrology/egr058

Koutsovitis P, Magganas A, Pomonis P and Ntaflos T (2013) Subduction-related rodingites from East Othris, Greece: Mineral reactions and physicochemical conditions of formation. Lithos 172-173: 139-157 http://dx.doi.org/10.1016/j.lithos.2013.04.009

Kretz R (1983) Symbols for rock-forming minerals. American Mineralogist 68: 277 - 279

Kurat, G, Palme H, Embey-Isztin A, Touret J, Ntaflos T, Spettel B, Brandstätten F, Palme C, Dreibus G and Prinz M (1993) Petrology and geochemistry of peridotites and associated vein rocks of Zabargad Island, Red Sea, Egypt. Earth and Environmental Science, Mineralogy and Petrology 48: 309-341 https://doi.org/10.1007/BF01163106

Lahondère D and Maurizot P (2009) Typologie et protocole d'échantillonnage des occurrences naturelles d'amiante en Nouvelle-Calédonie. Rapport BRGM/RP-57334-FR, 164 p.

Lahondère D, Cagnard F, Lahfid A, Wille G, Maurizot P (2011) L'amiante dans les massifs de péridotite de Nouvelle-calédonie. Rapport BRGM/RP-59252-FR, Rapport final, 302 p.

Lahondère D, Lesimple S, Cagnard F, Lahfid A, Wille G and Maurizot P (2012) Serpentinisation et fibrogenèse dans les massifs de péridotite de Nouvelle-Calédonie. Rapport BRGM/RP-60192-FR, CNRT Nickel et son environnement ; Amiante program, final report, 458 p.

Leake BE (1968) A catalog of analyzed calciferous and subcalciferous amphiboles together with their nomenclature and associated minerals. Geological Society of America Special Paper 98.

Leake BE, Woolley AR, Arps CES, Birch WD, Gilbert MC, Grice JD, Hawthorne,FC, Kato A, Kisch HJ, Krivovichev VG, Linthout K, Laird J, Mandarino JA, Maresch WV, Nickel EH, Rock NMS, Schumacher JC, Smith DC, Stephenson NVN, Ungaretti L, Whittaker EJW and Youzhi G (1997) Nomenclature of amphiboles. American Mineralogist 82: 1019-1037

Leguéré J (1976) Des corrélations entre la tectonique cassante et l'altération supergène des péridotites de Nouvelle Calédonie. PhD thesis, Université de Montpellier, France, 161 p.

Lupker M, France-Lanord C, Galy V, Lave J, Gaillardet J, Gajurel AP, Guilmette C, Rahman M, Singh KS and Sinha R (2012) Predominant floodplain over mountain weathering of Himalayan sediments

(Ganga basin). Geochimica et Cosmochimica Acta 84: 410-432 https://doi.org/10.1016/j.gca.2012.02.001

Marchesi C, Garrido CJ, Godard M, Belley F and Ferré E (2009) Migration and accumulation of ultra-depleted subduction-related melts in the Massif du Sud ophiolite (New Caledonia). Chemical Geology 266: 171-186 https://doi.org/10.1016/j.chemgeo.2009.06.004

Marocchi M, Hermann J, Tropper P, Bargossi GM and Mair V (2010) Amphibole and phlogopite in "hybrid" metasomatic bands monitor trace element transfer at the interface between felsic and ultramafic rocks (Eastern Alps, Italy). Lithos 117: 135–148 https://doi.org/10.1016/j.lithos.2010.02.011

Maurizot P and Cluzel D (2014) Pre-obduction records of Eocene foreland basins in central New Caledonia (Southwest Pacific); an appraisal from surface geology and Cadart 1 borehole data. New Zealand Journal of Geology and Geophysics 57: 307-311 https://doi.org/10.1080/00288306.2014.885065

Maurizot P and Lesimple S (2012) Le jade de Nouvelle-Calédonie. Aspects géologiques, gemmologiques et archéologiques. Geological Survey of New Caledonia internal report, 24 p.

Maurizot P, Cluzel D, Patriat M, Collot J, Iseppi M, Lesimple S, Secchiari A, Bosch D, Montanini A, Macera P and Davies HL (in press a) The Eocene Subduction-Obduction Complex. In: Mortimer, N. (ed) New Caledonia: Geology, Geodynamic Evolution and Mineral Resources. Geological Society, London, Memoir, chapter 5

Maurizot P, Sevin B, Lesimple S, Bailly L, Iseppi M and Robineau B (in press b) Mineral resources and prospectivity of the ultramafic rocks of New-Caledonia. In: Mortimer, N. (ed) New Caledonia: Geology, Geodynamic Evolution and Mineral Resources. Geological Society, London, Memoir, chapter 10

McArthur JM, Howarth RJ and Shields GA (2012) Strontium Isotope Stratigraphy. In: Gradstein F, Ogg J, Schmitz M, Ogg G The Geologic Time Scale 2012. Elsevier https://doi.org/10.1016/B978-0-444-59425-9.00007-X

McCaffrey R, Zwick PC, Bock Y, Prawirodirdjo L, Genrich JF, Stevens CW, Puntodewo SSO and Subarya C (2000) Strain partitioning during oblique plate convergence in northern Sumatra: Geodetic and seismologic constraints and numerical modelling. Journal of Geophysical Research 105(B12): 28363–28376 https://doi.org/10.1029/1999JB900362

McLennan SM, Taylor SR, McCulloch MT and Maynard JB (1990) Geochemical and Nd-Sr isotopic composition of deep-sea turbidites: Crustal evolution and plate tectonic associations. Geochimica et Cosmochimica Acta 54: 2015-2050 https://doi.org/10.1016/0016-7037(90)90269-Q

McNulty B and Farber D (2002) Active detachment faulting above the Peruvian flat slab: Geology 30: 567–570 https://doi.org/10 .1130 /0091-7613 (2002)030 <0567: ADFATP>2 .0 .CO;2

940 Méheut M, Lazzeri M, Balan E and Mauri F (2010) First-principles calculation of H/D isotopic
941 fractionation between hydrous minerals and water. Geochimica and Cosmochimica Acta 74: 3874–
942 3882 https://doi.org/10.1016/j.gca.2010.04.020
943 Mével C (2003) Serpentinization of abyssal peridotites at mid-ocean ridges. Compte Rendus
944 Geoscience 335: 825–852. https://doi.org/10.1016/j.crte.2003.08.006
945 Monnin C, Chavagnac V, Boulart C, Ménez B, Gérard M, Gérard E, Pisapia C, Quéméneur M,
946 Erauso G, Postec A, Guentas-Dombrowski L, Payri C and Pelletier B (2014) Fluid chemistry of the low
947 temperature hyperalkaline hydrothermal system of Prony Bay (New Caledonia). Biogeosciences 11:
948 5687–5706 https://doi.org/10.5194/bg-11-5687-2014
949 Morishita T, Hara K, Nakamura K, Sawaguchi T, Tamura A, Arai S, Okino K, Takai K and Kumagai H
950 (2009) Igneous, alteration and exhumation processes recorded in abyssal peridotites and related
951 fault rocks from an oceanic core complex along the Central Indian Ridge. Journal of Petrology 50 (7):
952 1299-1325 https://doi.org/10.1093/petrology/egp025
953 Mothersole FE, Evans K and Frost BR (2017) Abyssal and hydrated mantle wedge serpentinised
954 peridotites: a comparison of the 15°20'N fracture zone and New Caledonia serpentinites.
955 Contribution to Mineralogy and Petrology 172: 69. https://doi.org/10.1007/s00410-017-1381-x
956 Moutte J and Paris JP (1977) Observations nouvelles sur le grand massif ultramafique du sud de
957 la Nouvelle-Calédonie. Bulletin du BRGM section IV, I-1977: 43-51
958 Münker C, Wörner G, Yogodzinski G and Churikova T (2004) Behaviour of high field strength
959 elements in subduction zones: constraints from Kamchatka-Aleutian arc lavas. Earth and Planetary
960 Science Letters 224: 275-293 https://doi.org/10.1016/j.epsl.2004.05.030
961 Murthy RV and Beiser E (1968) Strontium isotopes in ocean water and marine sediments.
962 Geochimica and Cosmochimica Acta 32: 1121–1126. https://doi.org/10.1016/0016-7037(68)90111-7
963 Ningthoujam PS, Dubey CS, Guillot S, Fagion A-S and Shukla DP (2012) Origin and serpentinization
964 of ultramafic rocks of Manipur Ophiolite Complex in the Indo-Myanmar subduction zone, Northeast
965 India. Journal of Asian Earth Sciences 50: 128–134. https://doi.org/10.1016/j.jseaes.2012.01.004
966 O'Hanley DS, Chernosky JV Jr. and Wicks FJ (1989) The stability of lizardite and chrysotile.
967 Canadian Mineralogist 27: 483-493.
968 Orloff O (1968) Etude géologique et géomorphologique des massifs d'ultrabasites compris entre
969 Houailou et Canala (Nouvelle Calédonie). PhD Thesis, University of Montpellier (France), 80p.
970 Padrón-Navarta JA, Hermann J, Garrido JC, López Sánchez-Vizcaíno V and Gómez-Pugnaire MT
971 (2010) An experimental investigation of antigorite dehydration in natural silica-enriched serpentinite.
972 Contributions to Mineralogy and Petrology 159: 25-42 https://doi.org/10.1007/s00410-009-0414-5
973 Padrón-Navarta JA, López Sánchez-Vizcaíno V, Hermann J, Connolly JAD, Garrido JC, Gómez-
974 Pugnaire MT and Marchesi C (2013) Tschermak's substitution in antigorite and consequences for

phase relations and water liberation in high-grade serpentinites. Lithos 178: 186–196 https://doi.org/10.1016/j.lithos.2013.02.001

Paquette JL and Cluzel D (2007) U-Pb zircon dating of post-obduction volcanic-arc granitoids and a granulite-facies xenolith from New Caledonia. Inference on Southwest Pacific geodynamic models. International Journal of Earth Sciences (Geol. Rundsch.) 96: 613–622 https://doi.org/10.1007/s00531-006-0127-1

Paulick H, Bach W, Godard M, De Hoog JCM, Suhr G and Harvey J (2006) Geochemistry of abyssal peridotites (Mid-Atlantic Ridge, 15°20'N, ODP Leg 209): Implication for fluid/rock interaction in slow spreading environments. Chemical Geology 234: 179–210. https://doi.org/10.1016/j.chemgeo.2006.04.011

Pearce JA (1982) Trace element characteristics of lavas from destructive plate margins. In Thorpe R. S. (ed.). Andesites, John Wiley, Winchester pp. 528–548

Pearce JA, Lippard SJ and Roberts S (1984) Characteristics and tectonic significance of supra-subduction zone ophiolites. Geological Society, London, Special Publications 16: 77-94 https://doi.org/10.1144/GSL.SP.1984.016.01.06

Pelletier B (1996) Serpentines in nickel silicate ore from New Caledonia. Nickel 96 Conference, Kalgoorlie, Western Australia. Expanded abstracts volume: 197-206

Pirard C, Hermann J and O'Neil StC (2013) Petrology and geochemistry of the crust-mantle boundary in a nascent arc, Massif du Sud Ophiolite, New Caledonia, SW Pacific. Journal of Petrology 54: 1759-1792 https://doi.org/10.1093/petrology/egt030

Pollard DD and Segall P (1987) Chapter 8: Theoretical Displacements and Stresses Near Fractures in Rock: With Applications to Faults, Joints, Dikes, and Solution Surfaces, in Fracture Mechanics of Rock, B. Atkinson, ed., Academic Press, London, pp. 277-349

Prinzhoffer A (1981) Structure et pétrologie d'un cortège ophiolitique: le Massif du Sud (Nouvelle Calédonie): la transition manteau-croûte en milieu océanique. PhD Thesis École Nationale Supérieure des Mines de Paris, France. 185 p.

Python M, Yoshikawa M, Shibata T and Arai S (2011) Diopsidites and Rodingites: Serpentinisation and Ca-Metasomatism in the Oman Ophiolite Mantle. In: Dyke Swarms: Keys for Geodynamic Interpretation. Springer, Berlin, Heidelberg. https://doi.org/10.1007/978-3-642-12496-9_23

Quesnel B, Boulvais P, Gautier P, Cathelineau M, John CM, Dierick M, Agrinier P and Drouillet M (2016) Paired stable isotopes (O, C) and clumped isotope thermometry of magnesite and silica veins in the New Caledonia Peridotite Nappe. Geochimica et Cosmochimica Acta 183: 234–249 https://doi.org/10.1016/j.gca.2016.03.021

Quesnel B, Gautier P, Boulvais Ph, Cathelineau M, Maurizot P, Cluzel D, Ulrich M, Guillot S, Lesimple S and Couteau C (2013) Syn-tectonic, meteorite water-derived carbonation of the New Caledonia peridotite nappe. Geology 41: 1063–1066 https://doi.org/10.1130/G34531.1

1011 Quesnel B, Gautier P, Cathelineau M, Boulvais P, Couteau C and Drouillet M (2016) The internal
1012 deformation of the Peridotite Nappe of New Caledonia: A structural study of serpentine-bearing
1013 faults and shear zones in the Koniambo Massif. Journal of Structural Geology 85: 51–67
1014 https://doi.org/10.1016/j.jsg.2016.02.006
1015 Rivizzigno P, Lebon GT, Roe KK, Schrenk MO, Olson EJ, Lilley MD, Butterfield DA, Früh-Green GL
1016 and Blackman DK (2001) An off-axis hydrothermal vent field near the Mid-Atlantic Ridge at 30° N.
1017 Nature 412: 145-149 https://doi.org/10.1038/35084000
1018 Rodgers KA (1973a) Uralites and uralitization in the ultramafic belt of southern New Caledonia.
1019 Geological Magazine, G.B., 110: 125-131
1020 Rodgers KA (1973b) Felsic plutonic rocks from the southern portion of the New Caledonian
1021 ultramafic belt. Geological Magazine, G.B. 110: 431-446
1022 Rodgers KA and Bevan JC (1974) Hornblendites from the southern portion of the New Caledonian
1023 ultramafic belt. Mineralogical Magazine G.B., 39: 890-893.
1024 Rubatto D and Hermann J (2003) Zircon formation during fluid circulation in eclogites (Monviso,
1025 Western Alps): implications for Zr and Hf budget in subduction zones. Geochimica et Cosmochimica
1026 Acta 67: 2173–2187 https://doi.org/10.1016/S0016-7037(02)01321-2
1027 Rutter EH (1983) Pressure solution in nature, theory and experiment. Journal of the Geological
1028 Society, 140: 725-740 https://doi.org/10.1144/gsjgs.140.5.0725
1029 Schmidt K, Koschinsky A, Garbe-Schönberg D, de Carvalho LM and Seifert R (2007) Geochemistry
1030 of hydrothermal fluids from the ultramafic-hosted Logatchev hydrothermal field, 15°N on the Mid-
1031 Atlantic Ridge: temporal and spatial investigation. Chemical Geology 242: 1–21
1032 https://doi.org/10.1016/j.chemgeo.2007.01.023
1033 Schwartz S, Guillot S, Reynard B, Lafay R, Debret B, Nicollet C, Lanari P and Auzende AL (2013)
1034 Pressure-temperature estimates of the lizardite/antigorite transition in high pressure serpentinites.
1035 Lithos 178: 197–210 https://doi.org/10.1016/j.lithos.2012.11.023
1036 Secchiari A (2016) Geochemical and Sr, Nd, Pb isotope investigation of the New Caledonia
1037 ophiolite. Co-tutored PhD Thesis, University of Parma (Italy) and University of Montpellier (France),
1038 188 p.
1039 Secchiari A, Montanini A, Bosch D, Macera P and Cluzel D (2016) Melt extraction and enrichment
1040 processes in the New Caledonia lherzolites: evidence from geochemical and Sr-Nd isotope data.
1041 Lithos 260: 28-43 https://doi.org/10.1016/j.lithos.2016.04.030
1042 Secchiari A, Montanini A, Bosch D, Macera P and Cluzel D (2018) The contrasting geochemical
1043 message from the New Caledonia gabbronorites: insights on depletion and contamination processes
1044 of the sub-arc mantle in a nascent arc setting. Contributions to Mineralogy and Petrology 173: 66
1045 https://doi.org/10.1007/s00410-018-1496-8

Secchiari A, Montanini A, Bosch D, Macera P and Cluzel D (2019) Sr, Nd, Pb and trace element systematics of the New Caledonia harzburgites: tracking source depletion and contamination processes in a SSZ setting. Geosciences Frontiers (special issue on Ophiolites). https://doi.org/10.1016/j.gsf.2019.04.004

Siivola J and Schmid R (2007) Recommendations by the IUGS Subcommission on the Systematics of Metamorphic Rocks: Web version 01.02.07 www.bgs.ac.uk/scmr/home.html

Sivell W J and Waterhouse J B (1986) The geochemistry, origin, and tectonic significance of rodingites from the Dun Mountain Ultramafics, D'Urville Island, New Zealand. New Zealand Journal of Geology and Geophysics 29: 9-27 https://doi.org/10.1080/00288306.1986.10427519

Soret M, Agard P, Dubacq B, Vitale-Brovarone A, Monié P, Chauvet A, Whitechurch H and Villemant B (2016) Strain localization and fluid infiltration in the mantle wedge during subduction initiation: Evidence from the base of the New Caledonia ophiolite. Lithos 244: 1-19 https://doi.org/10.1016/j.lithos.2015.11.022

Trotet F, Kadar M and Marini D (2015) Typology of the New Caledonian Ni-laterite deposits: from natural to industrial processes. The Society for Geology Applied to Mineral Deposits, 13th SGA meeting, August 2015, Nancy, France. Abstr. vol.

Ulrich M (2010) Péridotites et serpentinites du complexe ophiolitique de la Nouvelle-Calédonie. Études pétrologiques, géochimiques et minéralogiques sur l'évolution d'une ophiolite de sa formation à son altération. Co-tutored PhD thesis, University of New Caledonia and University Joseph Fourier (Grenoble, France), 273 p.

Ulrich M, Bureau S, Chauvel C and Picard C (2012) Accurate Measurement of Rare Earth Elements by ICP-MS after Ion-Exchange Separation: Application to Ultra-Depleted Samples. Geostandards and Geoanalytical Research, 36: 7-20 https://doi.org/10.1111/j.1751-908X.2011.00116.x

Veizer J (1989) Strontium isotopes in seawater through time. Annual Review of Earth and Planetary Sciences 17: 141-167

Wang X, Zeng Z and Chen J (2009) Serpentinization of peridotites from the southern Mariana forearc. Progress in Natural Science 19: 1287–1295.

Wenner DB and Taylor HP Jr (1971) Temperatures of serpentinization of ultramafic rocks based on O^{18}/O^{16} fractionation between coexisting serpentine and magnetite. Contributions to Mineralogy and Petrology 32: 165-185 https://doi.org/10.1007/BF00643332

Wenner DB and Taylor HP Jr (1974) D/H and O^{18}/O^{16} studies of serpentinization of ultramafic rocks. Geochimica et Cosmochimica Acta 38: 1255-1286 https://doi.org/10.1016/0016-7037(74)901203

1080 Woodhead J, Hergt J, Greig A and Edwards L (2011) Subduction zone Hf-anomalies: mantle
1081 messenger, melting artefact or crustal process? Earth and Planetary Science Letters 304: 231–239
1082 https://doi.org/10.1016/j.epsl.2011.01.036
1083 Zheng YF (1993) Calculation of oxygen isotope fractionation in hydroxyl-bearing silicates. Earth
1084 and Planetary Science Letters 120: 247-263 https://doi.org/10.1016/0012-821X(93)90243-3
1085

Figure captions

Figure 1: Geological sketch map of New Caledonia.

Figure 2: a: Unserpentinized peridotite with olivine grains crosscut by cooling (?) micro-cracks (Kopeto mine). b: incipiently serpentinized peridotite with development of lizardite along parallel joints (Me Maoya Massif). c: outcrop picture and conceptual model (d) of centripetal development of 'primary' serpentinization (lizardite) in blocks of harzburgite delineated by a pre-existing joint network (roadside near Poro mine, east coast). Ol: olivine; Chr: chromite; Lz: lizardite

Figure 3: Tremolite-antigorite veins. a: mixed (successive ?) development of palisadic and radiating structures in a composite tremolite vein (Poro mine); b: antigorite crack seal developed against older lizardite-coated fracture walls; c: tension crack filled with tremolite crack seal; 3d: thin section of small-scale shear joint (micro-fault) showing oblique synkinematic tremolite fibres, note the chronological relationship of light brown lizardite veins (1) and tremolite crack seal (2). Tr: tremolite; Lz: lizardite; Atg: antigorite; Hzb: harzburgite

Figure 4: Outcrop picture (a) and conceptual model (b) of relationships between pressure solution, shear solution, and synkinematic crystal growth in tension and shear (pull apart) cracks. c: shear fracture (micro-fault) filled with syn-kinematic antigorite fibres (Atg) nucleated on pre-existing lizardite (Lz), magnetite grains (Mag) were formed by Fe liberation during syn-tectonic decomposition of lizardite; d: same features as c to show prominent magnetite formation (dark seams and streaks) at the boundary of newly formed antigorite (Atg) and pre-existing lizardite.

Figure 5: Microphotographs of synchronously crystallizing hydrous silicates in tension cracks of partly serpentinized peridotite. a-b: intergrowths of tremolite, antigorite and Mg-chlorite in a tension crack (a: planar light; b: crossed nicols). c-d: border of a tension crack showing syn-crystallizing tremolite and antigorite nucleated against lizardite of the wall rock (c: planar light; d: crossed nicols). Tr: tremolite; Chl: chlorite; Atg: antigorite; Lz: lizardite; Ol: olivine.

Figure 6: SEM image of intimately intergrown tremolite (Tr) and antigorite (Atg) fibres (sample# NC581DLA)

Figure 7: Raman spectra of tremolite and antigorite from sample# NC581DLA (see Fig. 6). Intensity is given in arbitrary units (a.u.).

Figure 8: Comparison of chondrite-normalized REE patterns (Evensen et al. 1978) to show the hook shape and relatively high REE contents of tremolite veins compared to New Caledonia peridotites (Secchiari 2016), early Eocene dykes (Cluzel et al. 2006) and serpentinites of the tectonic sole (with negative Ce anomaly; Ulrich, 2010)

Figure 9: Chemical classification (Leake, 1968; Leake et al. 1997) of microprobe analyses of single minerals from tremolite-bearing veins and pockets; the data form a continuous array spanning from high-Si tremolite to tremolite hornblende.

Figure 10: Hydrothermal incorporation of Cr in tremolite. a: Cr vs. Si plot of tremolite showing the increasing Cr molecular content with decreasing total Si content at increasing temperature (from tremolite to tremolite-hornblende. b: Cr_2O_3 (wt%) and X_{FeA} covariation similarly showing the positive correlation of Cr content and Fe ratio of tremolite.

Figure 11: a: Plot of Sr vs. $^{87}Sr/^{86}Sr$ to compare Sr isotopic composition of tremolite and antigorite (this study) to unserpentinized peridotites (Secchiari et al. 2018, 2019), gabbronorites (Secchiari et al. 2016), Early Eocene dykes (Cluzel et al. 2006) from the Peridotite Nappe, and Atlantis Massif serpentinites (Boschi et al. 2008). Ocean waters compositions are from Murthy and Beiser 1968, Elderfield (1986), Veizer (1989) and McArthur et al. (2012); b: plot of Ca vs. $^{87}Sr/^{86}Sr$, same symbols as in 11a.

Figure 12: $\delta^{18}O$ and δD isotopic ratios of fibrous serpentines and tremolites of Poro site. “Oceanic” serpentinites after Agrinier et al. (1995, 1997); supergene silicates field (“garnierite”) after Amisse et al. (2010) and deweylite after Wenner and Taylor (1974), serpentinite sole of the Peridotite Nappe after Ulrich (2010).

Figure 13: a: SEM image of altered chromite grain from peridotite isolated within a tremolite-antigorite replacive “vein”. The grain is formed of a residual core of primary chromite and a cortex of micro-granular chromian magnetite and low-Cr chromite. b & c sketch drawing to show the metasomatic replacement of peridotite wall rock by a mixture of tremolite and antigorite with partly altered chromite

Figure 14: Geodynamic model of subduction inception showing the timing of tremolite-antigorite veins development.

Table 1: Raman shift data from Raman spectra of two samples of tremolite-antigorite veins from Poro mine (data from Lahondere et al. 2012) uncertainty is ±2cm^{-1}

Table 2: Whole rock major and trace-elements composition of representative tremolite-antigorite veins of Poro Ni mine

Table 3: Microprobe analyses of tremolites

Table 4: Strontium isotopic data for tremolite-antigorite and antigorite veins from Poro Ni mine (east coast New Caledonia). $^{87}Sr/^{86}Sr$ normalization value = 0.710245

Table 5: Oxygen and hydrogen isotopic compositions of fibrous veins from Poro nickel mine (east coast New Caledonia)

1169 Table 1: Raman shift data from Raman spectra of two samples of tremolite-antigorite veins from
1170 Poro mine (data from Lahondere et al. 2012) uncertainty is ±2cm-1
1171
1172

NC225DL(2)-B	**NC226DL**	**NC225DL(2)-B**	**NC226DL**
Tremolite	Tremolite	Antigorite	Antigorite
124	-	-	-
164	166	233	233
181	184	-	-
226	227	381	378
372	375	-	-
398	395	-	-
419	-	-	-
532	-	687	691
656	-	1047	1046
676	676	-	-
751	-	3666	3666
933	-	3698	3699
1031	1032		
1066	1066		
3663	3662		
3676	3676		

1173 Table 2: Major and trace elements compositions of tremolite-antigorite bearing rocks and veins

sample	POR1a	POR1b	POR2a	POR2c	POR5	POR6	POR7b	POR 8c	POR10	POR 13
		Metasoma-		Tremol	Tremol					
	tremol	tized dyke	antigor?	mix	mix	tremol	tremol	antigor?	antigor	antigor?
SiO2	50.17	47.63	37.57	46.87	43.98	55.39	55.59	43.30	43.37	42.92
TiO2	< D.L.	13.30	0.06	< D.L.	< D.L.	< D.L.	< D.L.	< D.L.	< D.L.	< D.L.
Al2O3	1.73	13.32	6.12	1.08	0.59	1.87	1.40	0.06	0.06	0.62
Fe2O3	2.59	4.88	3.49	4.78	3.68	1.88	2.04	3.40	2.80	6.96
MnO	0.07	0.03	0.25	0.08	0.07	0.07	0.08	0.09	0.08	0.04
MgO	28.32	0.41	36.24	30.28	33.36	24.28	25.09	38.39	39.76	36.22
CaO	7.19	12.56	0.02	5.07	1.82	11.52	11.16	0.01	0.01	0.03
Na2O	0.51	5.30	< D.L.	0.30	0.11	0.55	0.40	< D.L.	< D.L.	0.01
K2O	< D.L.	0.05	< D.L.	< D.L.	< D.L.	< D.L.	< D.L.	< D.L.	< D.L.	< D.L.
P2O5	< D.L.	0.03	< D.L.	< D.L.	< D.L.	< D.L.	< D.L.	< D.L.	< D.L.	< D.L.
PF	8.03	1.78	15.88	10.57	14.94	3.85	3.89	14.42	14.18	12.76
Total	98.61	99.28	99.63	99.03	98.54	99.40	99.64	99.66	100.25	99.56
$^{87}Sr/^{86}Sr$	0.704262	0.704417	0.707058	0.704402	0.705369	0.703894	0.704239	0.706264	0.708290	0.702853
As	< D.L.	< D.L.	< D.L.	< D.L.	< D.L.	< D.L.	< D.L.	< D.L.	< D.L.	< D.L.
Ba	< D.L.	< D.L.	< D.L.	< D.L.	< D.L.	< D.L.	< D.L.	< D.L.	< D.L.	< D.L.
Be	< D.L.	< D.L.	< D.L.	< D.L.	< D.L.	< D.L.	< D.L.	< D.L.	< D.L.	< D.L.
Bi	< D.L.	< D.L.	< D.L.	< D.L.	< D.L.	< D.L.	< D.L.	< D.L.	< D.L.	< D.L.
Cd	0.321	0.161	< D.L.	0.136	< D.L.	< D.L.	< D.L.	< D.L.	< D.L.	0.302
Ce	1.929	2.39	< D.L.	1.236	0.918	1.66	1.323	< D.L.	< D.L.	1.348
Co	524.6	291.1	44.34	387.2	116.6	21.49	79.13	53.15	48.39	47.53
Cr	2915	3372	3335	2849	1589	2636	2448	42.99	169.1	2252
Cs	< D.L.	< D.L.	< D.L.	< D.L.	< D.L.	< D.L.	< D.L.	< D.L.	< D.L.	< D.L.
Cu	< D.L.	< D.L.	< D.L.	< D.L.	< D.L.	< D.L.	< D.L.	< D.L.	< D.L.	< D.L.
Dy	0.274	0.313	< D.L.	0.156	0.11	0.168	0.141	0.019	< D.L.	0.196
Er	0.174	0.198	< D.L.	0.092	0.07	0.133	0.108	0.01	< D.L.	0.122
Eu	0.162	0.192	< D.L.	0.092	0.065	0.138	0.113	0.006	< D.L.	0.12
Ga	1.095	1.1	1.69	0.741	0.459	1.362	1.053	0.345	0.447	0.896
Gd	0.297	0.327	< D.L.	0.173	0.118	0.166	0.123	0.024	< D.L.	0.189
Ge	1.379	1.431	0.423	1.398	1.104	1.716	1.691	1.071	1.076	1.114
Hf	0.033	0.036	< D.L.	< D.L.	< D.L.	< D.L.	< D.L.	< D.L.	< D.L.	0.056
Ho	0.058	0.066	< D.L.	0.03	0.024	0.039	0.032	0.004	< D.L.	0.041
In	< D.L.	< D.L.	< D.L.	< D.L.	< D.L.	< D.L.	< D.L.	< D.L.	< D.L.	< D.L.
La	0.538	0.642	< D.L.	0.324	0.575	0.444	0.344	< D.L.	< D.L.	0.337
Lu	0.029	0.032	< D.L.	0.013	0.012	0.029	0.024	< D.L.	0.002	0.02
Mo	< D.L.	< D.L.	< D.L.	< D.L.	1.007	< D.L.	< D.L.	< D.L.	< D.L.	0.731
Nb	< D.L.	< D.L.	0.121	< D.L.	< D.L.	< D.L.	< D.L.	< D.L.	< D.L.	< D.L.
Nd	1.358	1.644	< D.L.	0.894	0.737	0.912	0.765	0.105	< D.L.	0.906
Ni	6467	4102	1483	5357	15680	1729	3206	5063	1395	7830
Pb	< D.L.	< D.L.	< D.L.	< D.L.	< D.L.	< D.L.	< D.L.	< D.L.	< D.L.	< D.L.

1175

1176

sample	POR1a tremol	POR1b tremol	POR2a antigor?	POR2c tremol	POR5 tremol	POR6 tremol	POR7b tremol	POR 8c antigor?	POR10 antigor	POR 13 antigor?
Pr	0.33	0.394	< D.L.	0.203	0.198	0.251	0.198	0.025	0.012	0.224
Rb	< D.L.	< D.L.	< D.L.	< D.L.	< D.L.	< D.L.	< D.L.	< D.L.	< D.L.	< D.L.
Sc	13	< D.L.	< D.L.	25.39	13.29	10.86	11.87	< D.L.	< D.L.	< D.L.
Sb	< D.L.	< D.L.	< D.L.	< D.L.	< D.L.	< D.L.	< D.L.	< D.L.	< D.L.	< D.L.
Sm	0.321	0.365	< D.L.	0.196	0.135	0.186	0.149	0.026	< D.L.	0.211
Sn	< D.L.	< D.L.	< D.L.	< D.L.	< D.L.	< D.L.	< D.L.	< D.L.	< D.L.	< D.L.
Sr	6.963	7.57	< D.L.	3.947	< D.L.	14.19	7.77	< D.L.	< D.L.	3.968
Ta	< D.L.	< D.L.	0.018	< D.L.	< D.L.	< D.L.	< D.L.	< D.L.	< D.L.	< D.L.
Tb	0.047	0.055	< D.L.	0.027	0.02	0.028	0.021	< D.L.	< D.L.	0.031
Th	< D.L.	< D.L.	< D.L.	< D.L.	< D.L.	< D.L.	< D.L.	< D.L.	< D.L.	< D.L.
Tm	0.028	0.03	< D.L.	0.014	0.011	0.024	0.02	0.002	0.001	0.02
U	< D.L.	< D.L.	< D.L.	< D.L.	< D.L.	< D.L.	< D.L.	< D.L.	< D.L.	< D.L.
V	103.3	110.6	28.97	72.11	42.59	190.9	173.1	14.23	13.57	73.97
W	< D.L.	< D.L.	< D.L.	< D.L.	< D.L.	< D.L.	< D.L.	< D.L.	< D.L.	< D.L.
Y	1.734	1.885	< D.L.	0.833	0.647	1.108	0.951	< D.L.	< D.L.	1.154
Yb	0.194	0.22	< D.L.	0.091	0.08	0.178	0.148	0.008	0.008	0.139
Zn	97.97	52.38	< D.L.	54.83	22.71	< D.L.	23.35	17.43	16.71	< D.L.
Zr	1.533	1.765	< D.L.	< D.L.	< D.L.	< D.L.	< D.L.	< D.L.	< D.L.	2.458

1177

1178

1179

1180

1181 Table 3: microprobe analyses of tremolites

1182

Spot#	Na2O	MgO	SiO2	Al2O3	K2O	CaO	TiO2	Cr2O3	FeO	MnO	NiO	Total
87	0.504	23.918	56.915	1.412	0.000	12.453	0.000	0.38	1.593	0.086	0.013	97.275
88	1.042	22.125	54.209	3.489	0.017	11.725	0.045	0.901	2.142	0.000	0.171	95.865
89	0.801	23.956	56.247	2.415	0.049	12.307	0.000	0.732	1.737	0.003	0.082	98.329
1	0.19	24.867	58.846	0.378	0.018	13.291	0.000	0.061	1.108	0.073	0.145	98.977
12	0.009	24.539	58.69	0.08	0.002	13.463	0.029	0.086	1.025	0.006	0.153	98.081
21	0.904	23.675	55.909	2.864	0.051	12.282	0.082	0.195	1.914	0.15	0.082	98.107
22	0.804	23.614	54.598	2.766	0.006	12.381	0.000	0.714	1.879	0.024	0.283	97.068
23	0.184	24.552	58.604	0.473	0.006	12.956	0.025	0.003	1.26	0.114	0.236	98.412
24	0.255	24.571	57.662	0.598	0.002	12.913	0.000	0.048	1.406	0.000	0.179	97.634
25	0.722	23.759	56.39	2.132	0.000	12.798	0.000	0.627	1.647	0.129	0.095	98.299
27	0.231	24.425	58.317	0.605	0.072	13.249	0.031	0.126	1.195	0.000	0.124	98.376
28	0.768	24.121	56.579	2.116	0.002	12.369	0.000	0.168	1.865	0.084	0.211	98.284
34	1.063	24.586	50.703	2.29	0.05	11.555	0.000	0.61	1.721	0.126	0.262	92.967
36	0.298	25.178	57.362	0.533	0.000	11.859	0.046	0.237	2.183	0.157	0.159	98.011
37	0.731	23.781	56.45	2.202	0.000	12.512	0.000	0.522	1.83	0.033	0.047	98.108
38	0.71	23.563	56.467	2.263	0.05	12.477	0.036	0.522	1.682	0.000	0.024	97.794
39	1.254	23.265	54.974	4.231	0.041	11.967	0.091	0.735	2.583	0.134	0.064	99.34
40	0.565	23.974	56.975	1.938	0.023	12.617	0.017	0.402	1.708	0.001	0.000	98.218
42	1.036	23.633	53.843	3.516	0.015	12.027	0.000	1.233	2.307	0.000	0.000	97.612
48	1.04	23.518	54.855	3.351	0.011	12.173	0.012	0.768	2.039	0.115	0.074	97.957
49	1.141	23.469	54.485	3.629	0.012	12.311	0.078	0.796	2.123	0.138	0.112	98.294
50	0.665	23.907	56.915	1.97	0.043	12.684	0.000	0.352	1.529	0.184	0.129	98.378
53	0.914	23.647	55.907	2.844	0.053	12.298	0.032	0.539	1.963	0.018	0.136	98.352
54	1.163	22.896	53.848	3.769	0.014	12.004	0.000	0.825	2.163	0.135	0.301	97.119
55	1.17	23.237	54.081	3.487	0.021	12.375	0.000	0.629	2.16	0.108	0.021	97.289
56	0.962	23.511	55.354	3.152	0.002	12.383	0.000	0.606	2.183	0.102	0.25	98.505
59	1.047	23.452	54.974	3.265	0.006	12.539	0.000	0.544	1.897	0.116	0.159	97.999
80	0.735	23.803	55.714	2.296	0.000	12.616	0.034	0.648	1.648	0.121	0.19	97.805
82	0.68	23.865	56.148	2.267	0.002	12.407	0.000	0.67	1.782	0.008	0.182	98.012
83	0.522	29.048	51.846	1.628	0.015	8.143	0.000	0.491	2.593	0.08	0.226	94.593
85	0.969	23.976	55.769	2.777	0.015	12.058	0.008	0.77	2.019	0.037	0.216	98.614
96	0.864	23.749	55.321	2.717	0.035	12.513	0.048	0.833	1.704	0.111	0.000	97.895
97	0.647	25.043	57.255	1.912	0.000	10.987	0.000	0.507	2.293	0.09	0.085	98.818
98	0.746	24.14	56.104	2.259	0.055	12.465	0.007	0.656	1.68	0.061	0.213	98.388
99	0.573	24.48	57.347	1.641	0.026	12.188	0.045	0.57	1.656	0.094	0.004	98.623
107	0.192	25.294	57.056	0.575	0.027	12.034	0.058	0.201	2.166	0.165	0.15	97.918
111	0.7	24.236	56.928	2.031	0.017	12.5	0.000	0.605	1.583	0.000	0.216	98.816
112	1.034	23.895	55.36	3.147	0.025	11.606	0.074	0.793	1.72	0.022	0.026	97.701
114	0.693	24.658	56.873	1.904	0.023	11.447	0.000	0.453	2.245	0.181	0.111	98.587
131	1.041	23.147	54.364	3.395	0.019	12.352	0.000	0.895	1.887	0.136	0.032	97.267
132	0.539	24.785	55.089	2.585	0.021	11.722	0.000	0.599	1.736	0.013	0.123	97.212
133	0.245	28.133	55.568	0.359	0.008	9.6	0.000	0.092	1.516	0.159	0.000	95.679

134	0.17	30.601	51.269	2.507	0.009	7.19	0.000	0.307	1.718	0.111	0.102	93.984
135	0.174	27.053	56.341	0.243	0.04	10.506	0.03	0.095	1.533	0.036	0.013	96.066
149	0.22	25.962	56.11	0.594	0.000	11.748	0.009	0.189	1.724	0.079	0.084	96.72
150	1.457	22.342	52.332	5.442	0.032	12.595	0.027	1.189	2.16	0.144	0.024	97.743
175	0.006	24.879	58.634	0.049	0.000	13.236	0.000	0.013	1.361	0.015	0.203	98.396
184	0.065	24.378	58.639	0.167	0.014	12.87	0.000	0.16	1.64	0.073	0.04	98.047
185	0.573	24.648	56.837	1.682	0.022	12.041	0.000	0.481	1.861	0.135	0.381	98.662
186	0.557	24.127	56.995	1.924	0.017	12.753	0.000	0.51	1.774	0.045	0.024	98.724
187	0.712	24.163	56.97	2.167	0.05	12.293	0.000	0.559	1.988	0.041	0.23	99.174
188	0.44	25.599	56.112	1.463	0.000	10.51	0.000	0.396	1.747	0.082	0.738	97.086
189	0.715	24.465	56.55	2.379	0.000	12.155	0.000	0.661	1.774	0.000	0.083	98.782
190	0.655	24.285	56.226	2.24	0.047	11.875	0.000	0.659	2.028	0.174	0.516	98.705
191	0.64	27.375	54.089	2.1	0.003	9.989	0.000	0.604	2.485	0.019	0.291	97.596
192	0.796	23.771	55.874	2.474	0.059	12.275	0.000	0.654	1.917	0.000	0.164	97.984
194	0.575	25.642	57.97	1.873	0.04	9.999	0.047	0.568	2.58	0.183	0.106	99.583

1183

1184 Table 4 : Sr isotopic compositions of tremolite-antigorite veins

1185

sample	Field name	CaO wt%	Sr ppm	$^{87}Sr/^{86}Sr$
POR 1a	Tremolite mix	7.19	6.963	0.704262
POR 1b	metasomatized dyke	12.56	7.57	0.704417
POR 2a	antigorite ?	0.02	< DL	0.707058
POR 2c	Tremolite mix	5.07	3.947	0.704402
POR 5	Tremolite mix	1.82	< DL	0.705369
POR 6	tremolite	11.52	14.19	0.703894
POR 7b	tremolite	11.16	7.77	0.704239
POR 8c	antigorite ?	0.01	< DL	0.706264
POR 10	antigorite	0.01	< DL	0.708290
POR 13	antigorite ?	0.02	3.968	0.702853
Sr341	antigorite	0.002	0.058	0.709741
Sr343	tremolite	9.6	8.885	0.704207
Sr344	antigorite	0.002	0.086	0.709701
Sr346	antigorite	0.004	1.428	0.707945
Sr347	antigorite	0.002	0.036	0.709546
Sr349	antigorite	0.002	0.351	0.709687
Sr350	antigorite	0.002	0.070	0.710002
Sr353	antigorite	0.002	0.173	0.709261
Sr354	tremolite	4.675	5.250	0.704542
Sr355	antigorite ?	0.113	0.617	0.708086
Sr356	tremolite	9.422	9.239	0.704205
Sr357	antigorite	0.002	0.183	0.711584
Sr359	tremolite	5.248	4.318	0.704350
Sr360	tremolite	3.386	3.979	0.704529

1186

1187

1188 Table 5: Oxygen and hydrogen isotopic compositions

1189

			$\delta^{18}O$		δD	
sample.	location	Type	(‰ SMOW)	±	(‰ SMOW)	±
POR1a	Poro	tremolite	7.2	0.25	-58.3	1.2
POR1b	Poro	tremolite	7.2	0.25	-46.8	1.8
POR2a	Poro	tremolite	7.1	0.25	-82.8	2.2
POR2b	Poro	tremolite	6.2	0.25	-47.2	1.1
POR2c	Poro	tremolite	6.3	0.25	-45.3	1.4
POR3b	Poro	antigorite	6.3	0.25	-47.3	2.1
POR4	Poro	Mg-chlorite (penninite)	3.3	0.25	-17.5	2.9
POR5	Poro	tremolite	8.8	0.25	-60.6	3.9
POR6	Poro	tremolite (?)	6.5	0.25	-51.5	1.6
POR7b	Poro	tremolite (?)	5.2	0.25	-46.0	2.1
POR8	Poro	antigorite	6.3	0.25	-50.6	2.0
POR8b	Poro	antigorite	2.7	0.25	-41.8	3.0
POR8c	Poro	antigorite (?)	6.6	0.25	-52.7	2.1
POR10	Poro	antigorite	6.3	0.25	-40.4	1.0
POR12	Poro	antigorite	6.7	0.25	-45.7	1.1
POR14	Poro	slickensided porcelain-like serpentine	8.8	0.25	-105.8	0.9
POR15	Poro	porcelain-like serpentine in tensional crack seal	8.3	0.25	-107.7	1.1
VUL 4-1	Vulcain	weathered antigorite	4.5	0.25	-61.2	2.7
VUL 4-2	Vulcain	weathered antigorite	6.9	0.25	-107.2	0.4
VUL 4-3	Vulcain	unweathered antigorite	5.8	0.25	-38.7	4.8
VUL 4-4	Vulcain	slightly weathered antigorite	6.0	0.25	-42.1	2.0

1190

1191

1192

Figure 1

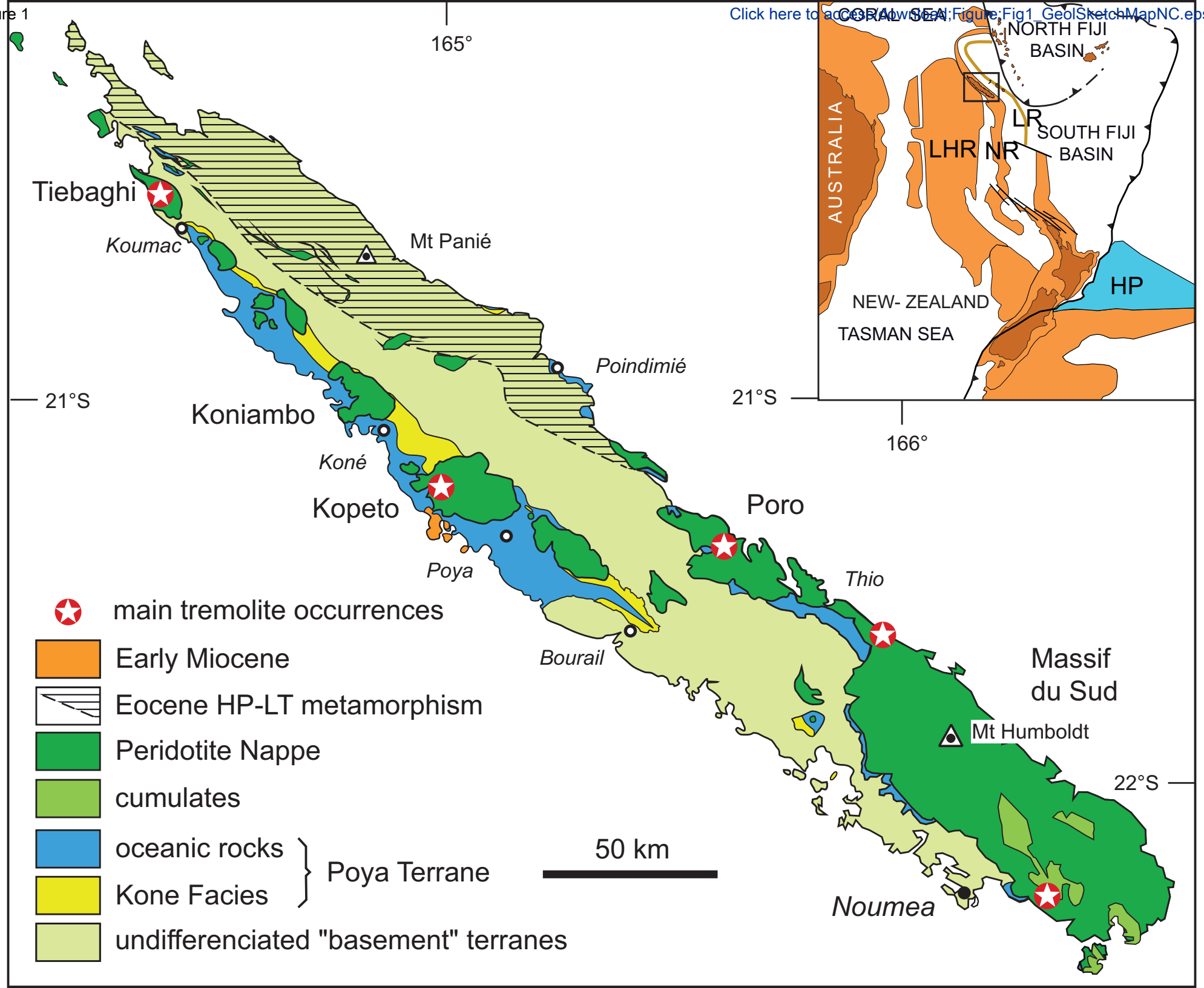

Figure 2

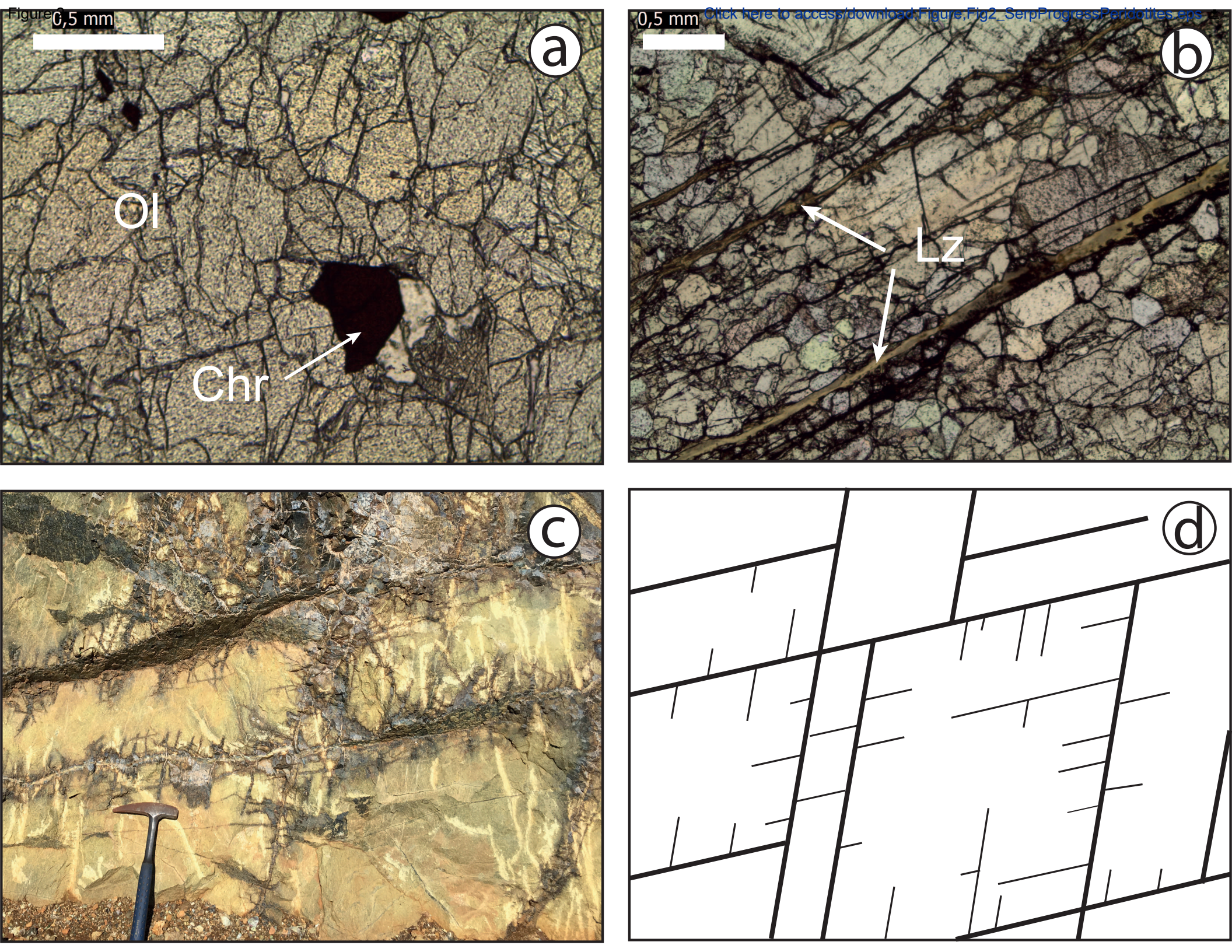

Figure 3

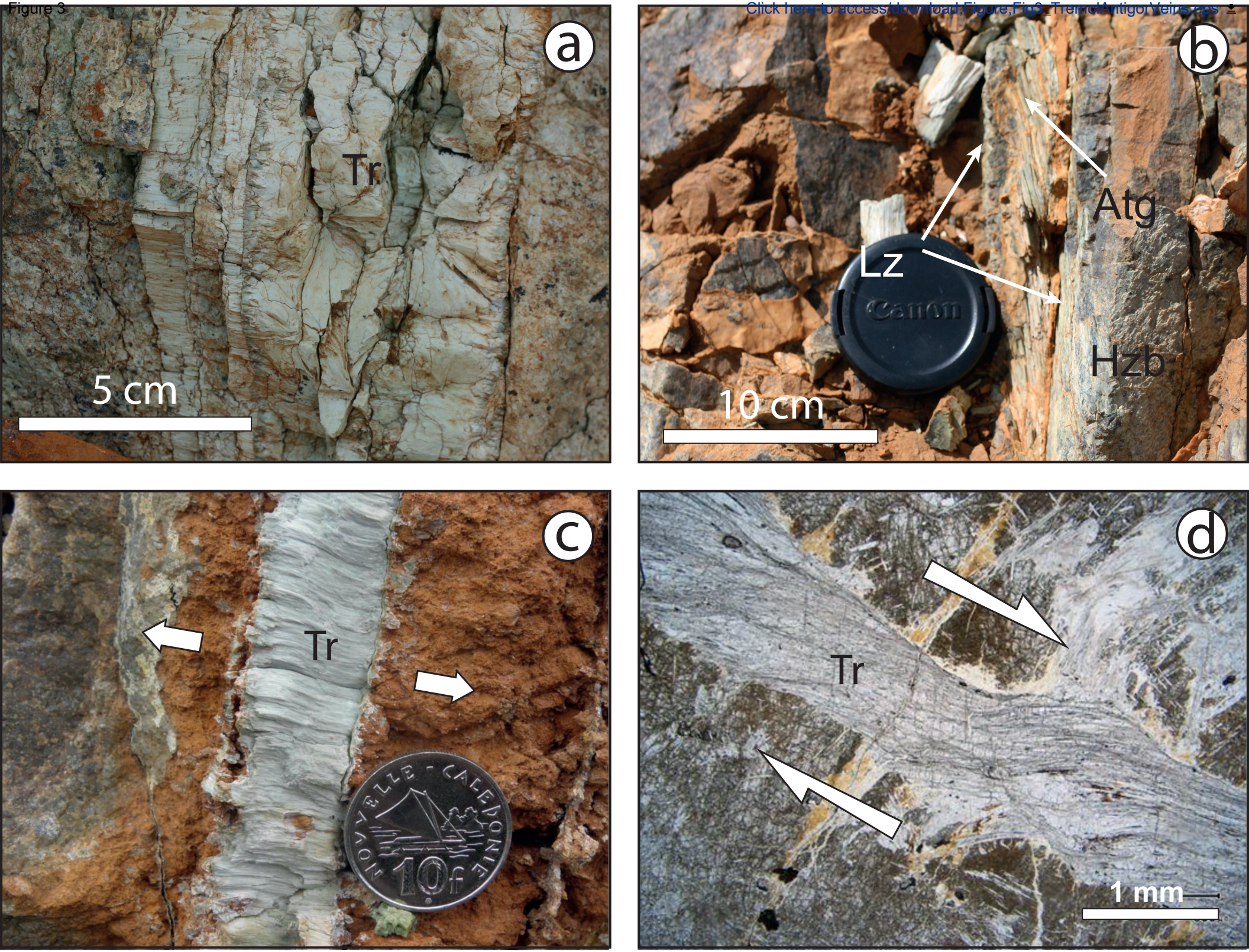

Figure 4

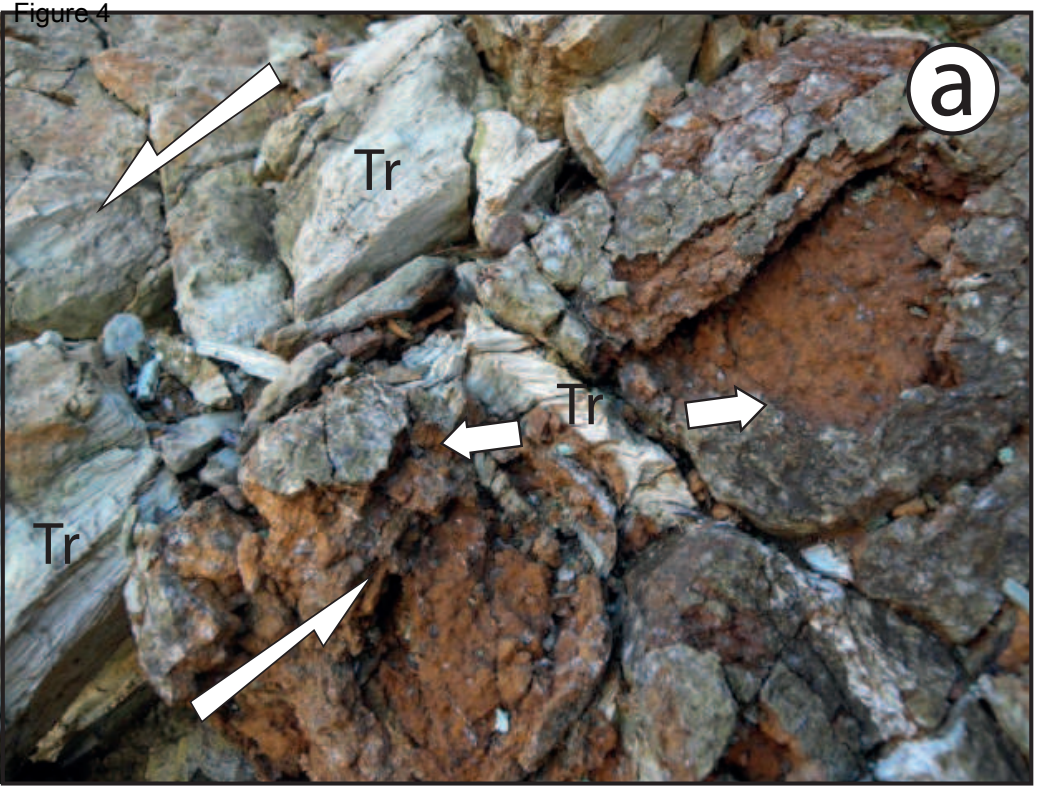

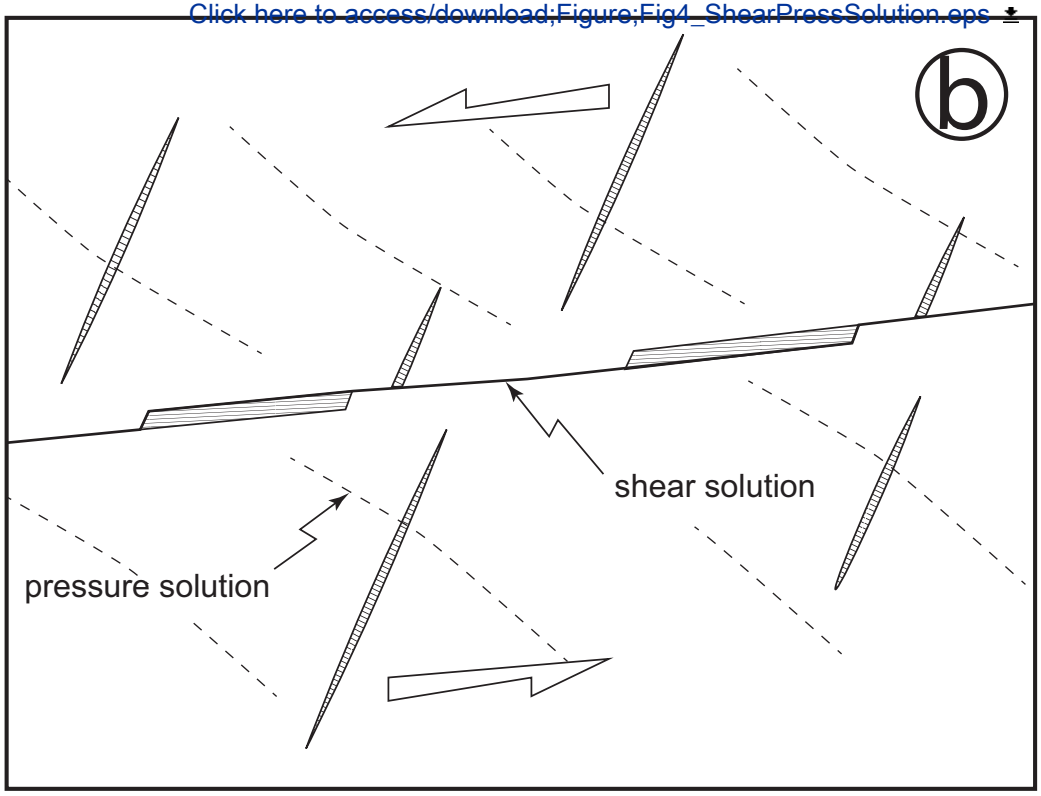

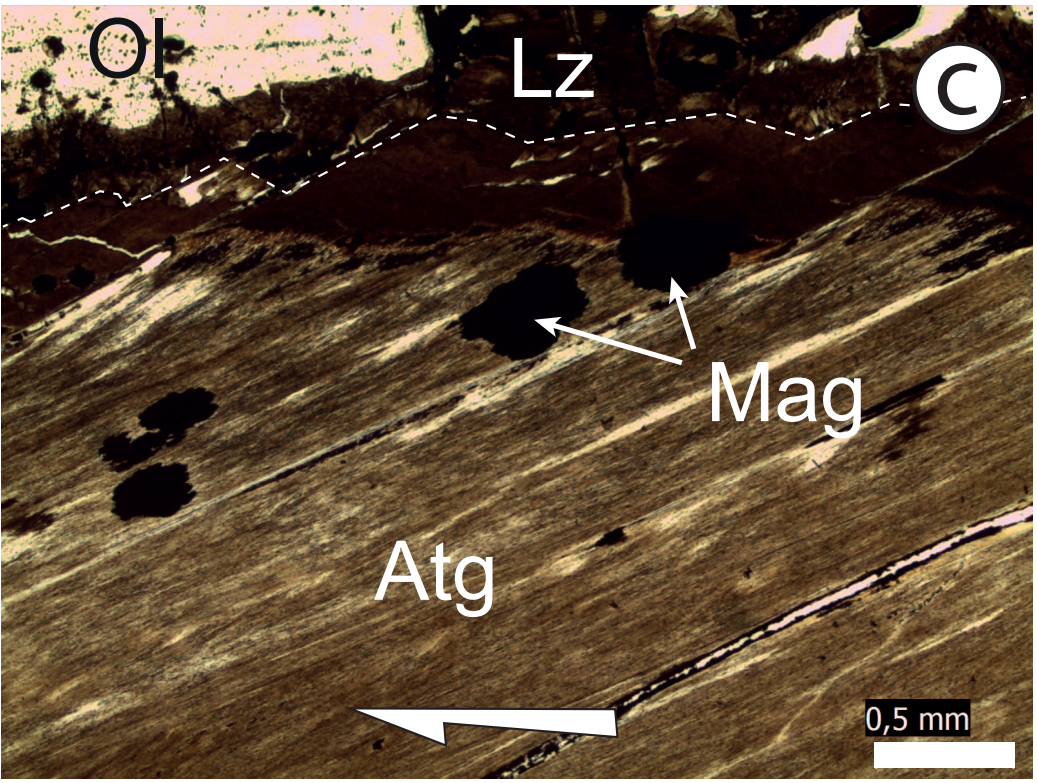

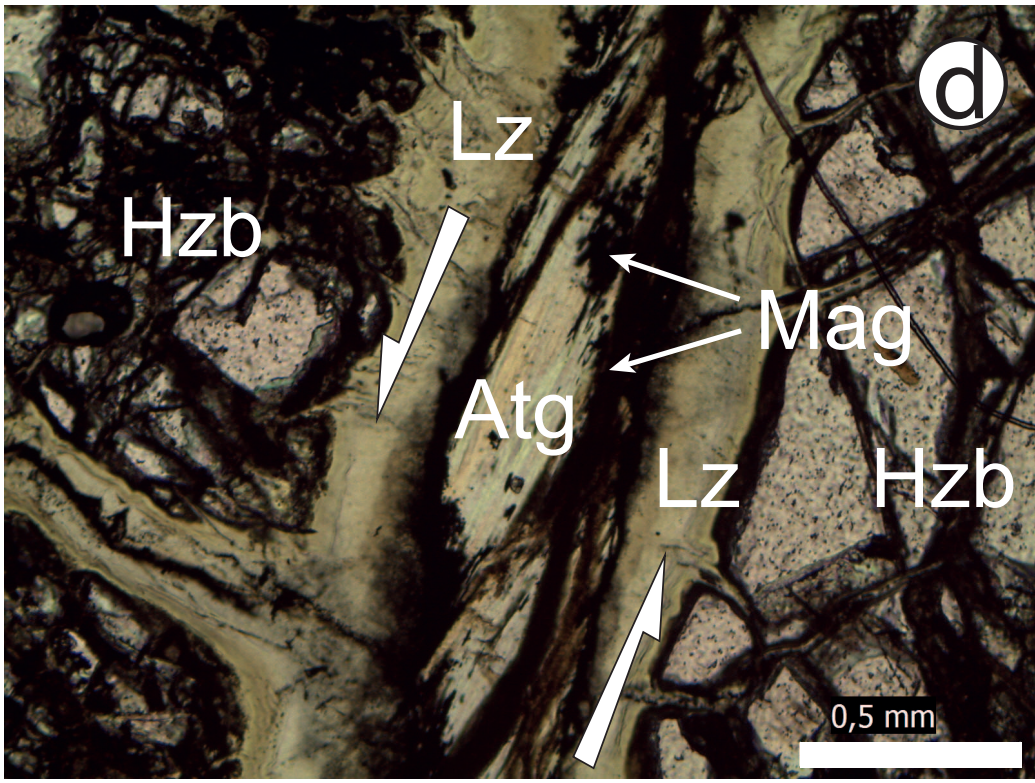

Figure 5

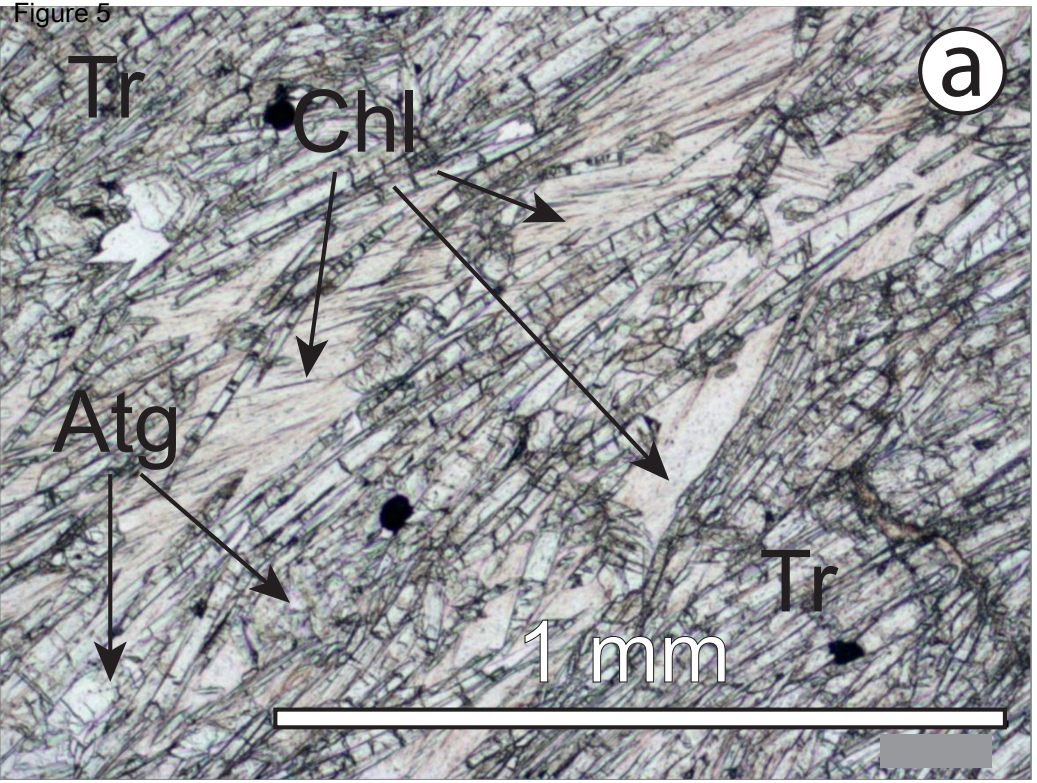

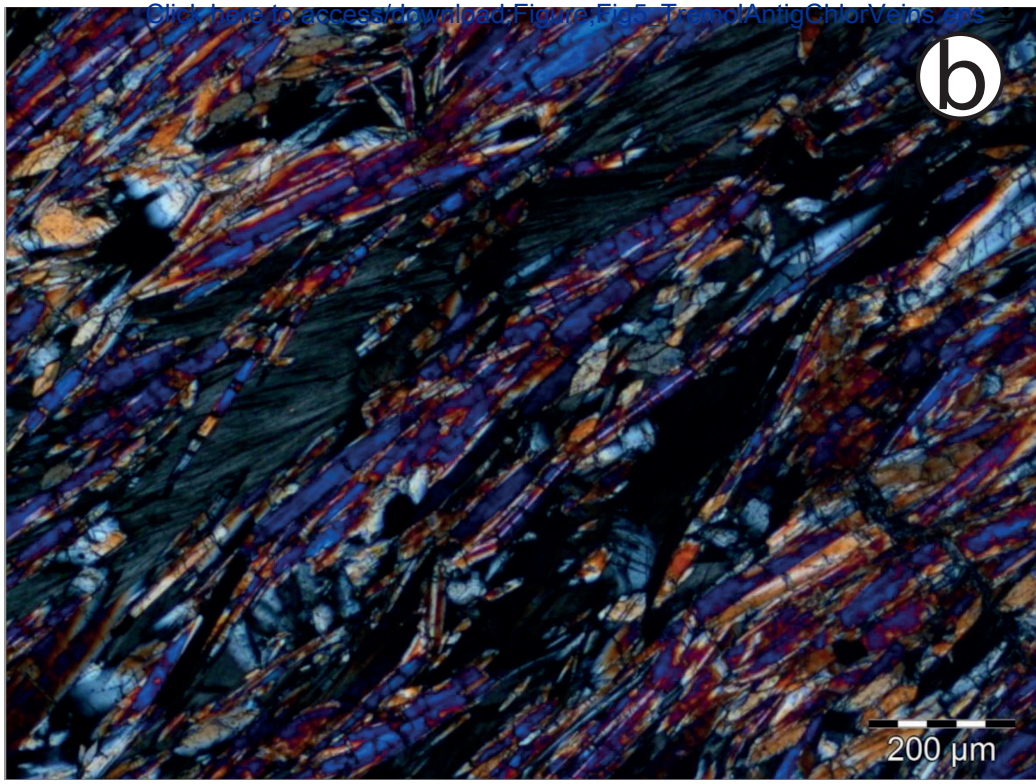

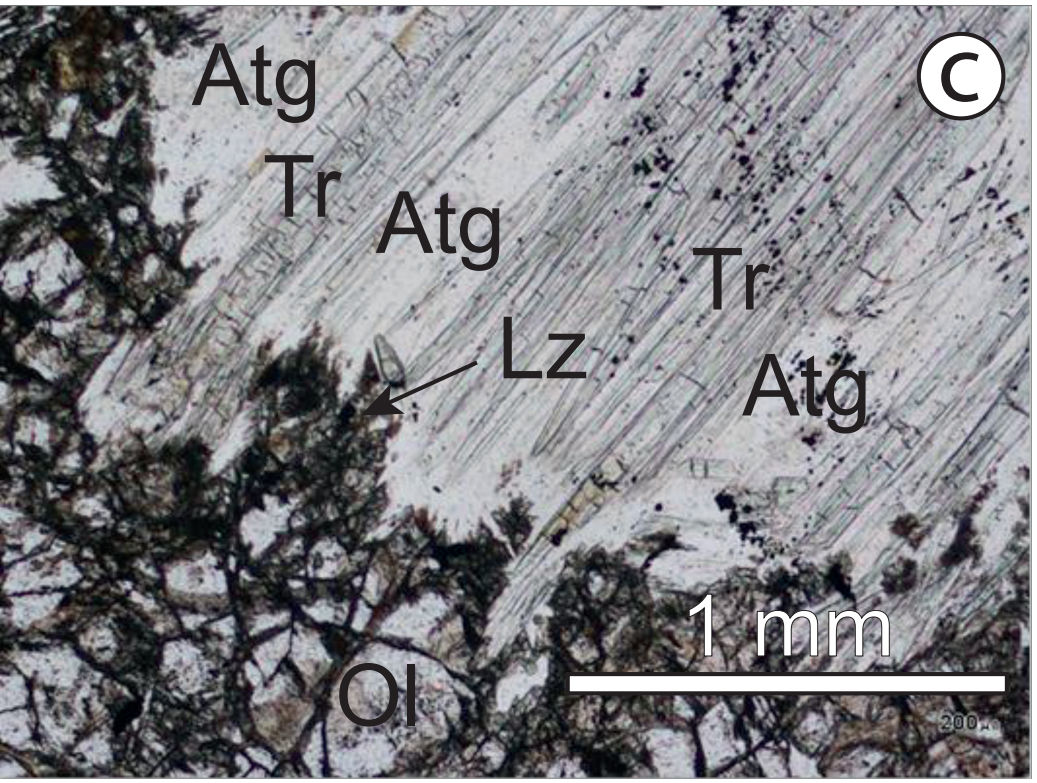

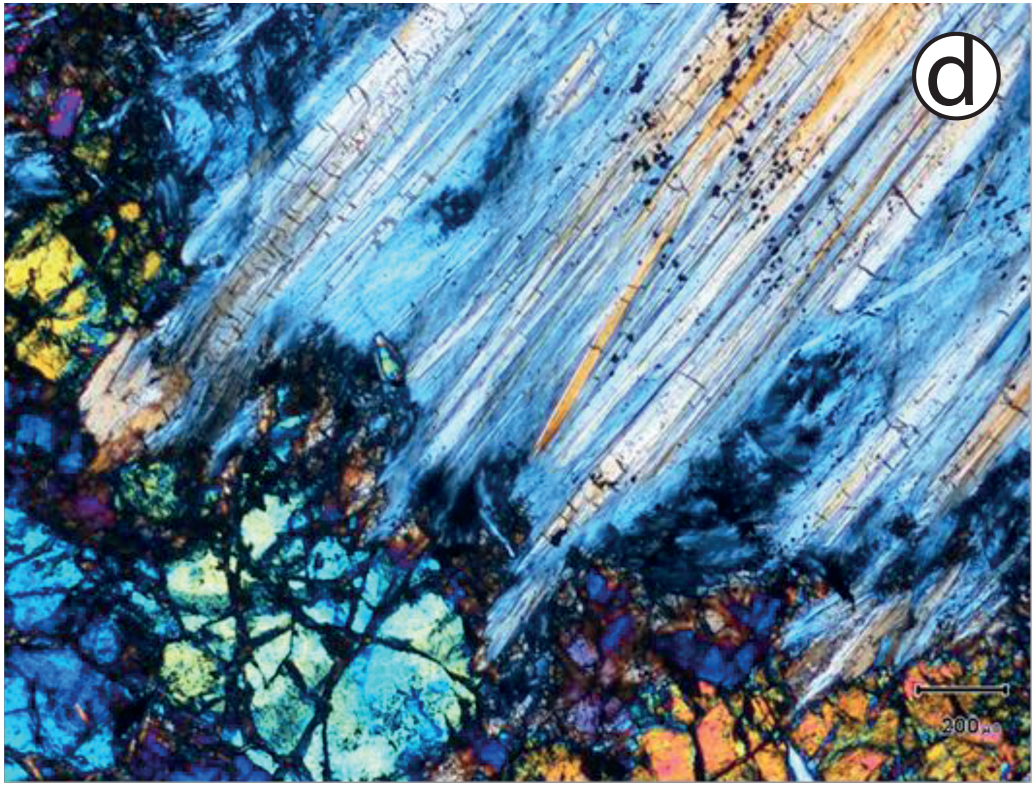

Figure 6

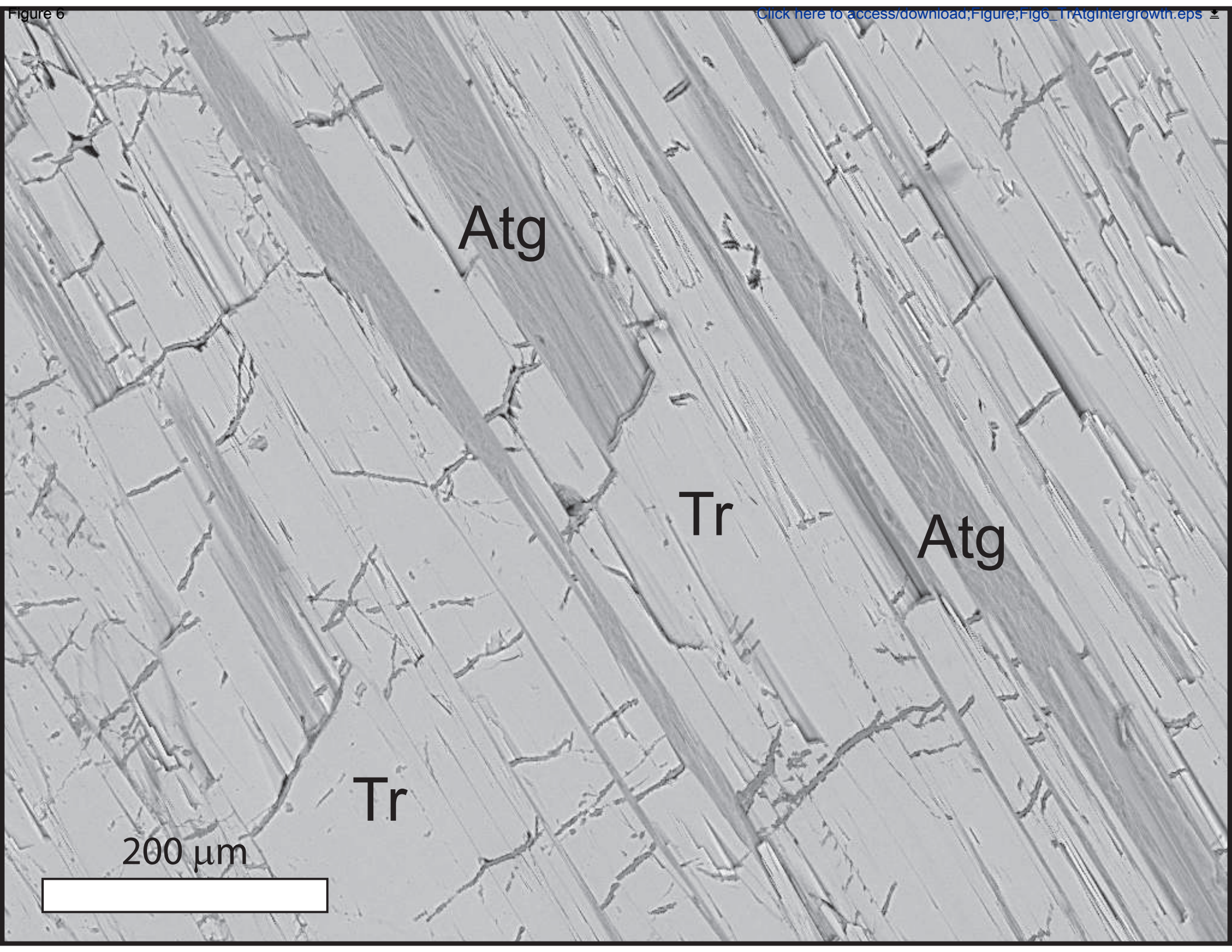

Figure 7

Click here to access/download;Figure;Fig7_RamanTremAntig.eps

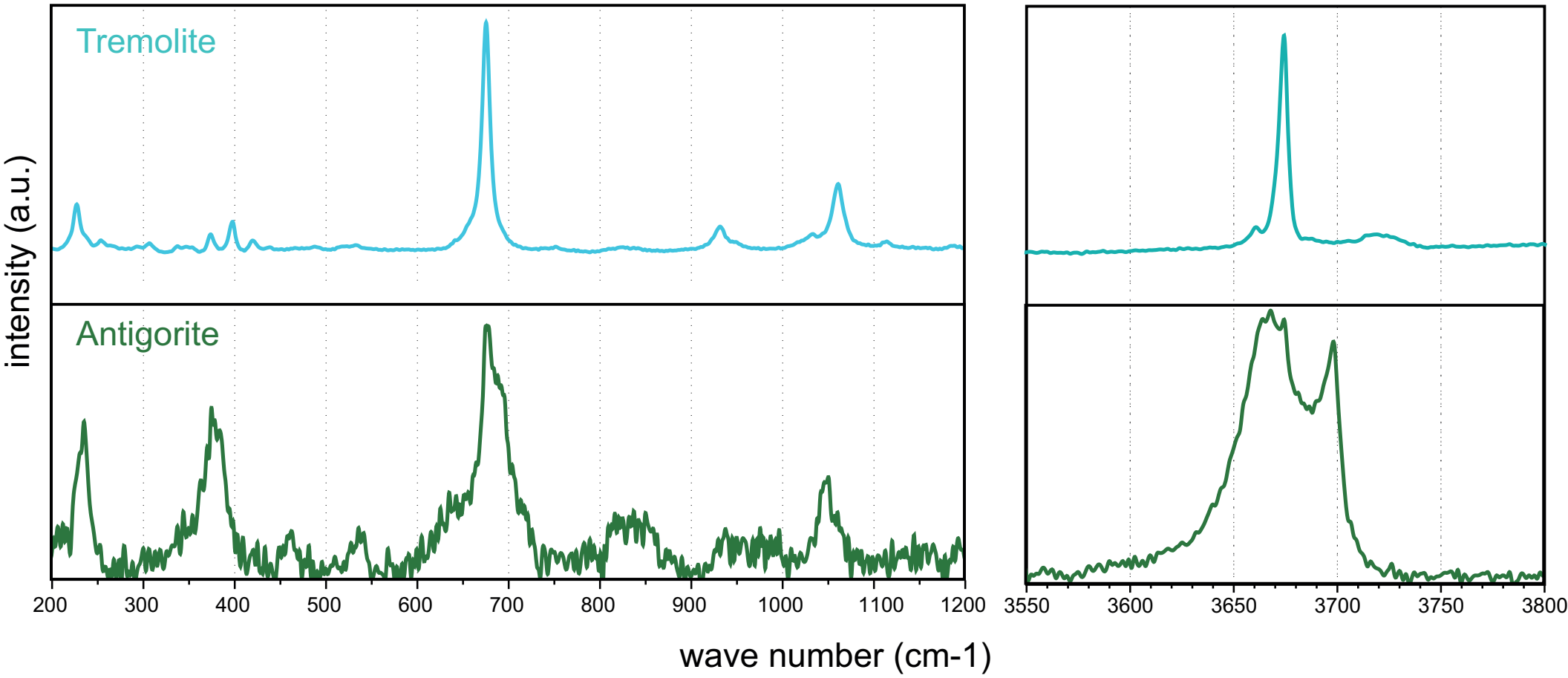

Figure 8

Click here to access/download;Figure;Fig8_REETremolDikes.eps

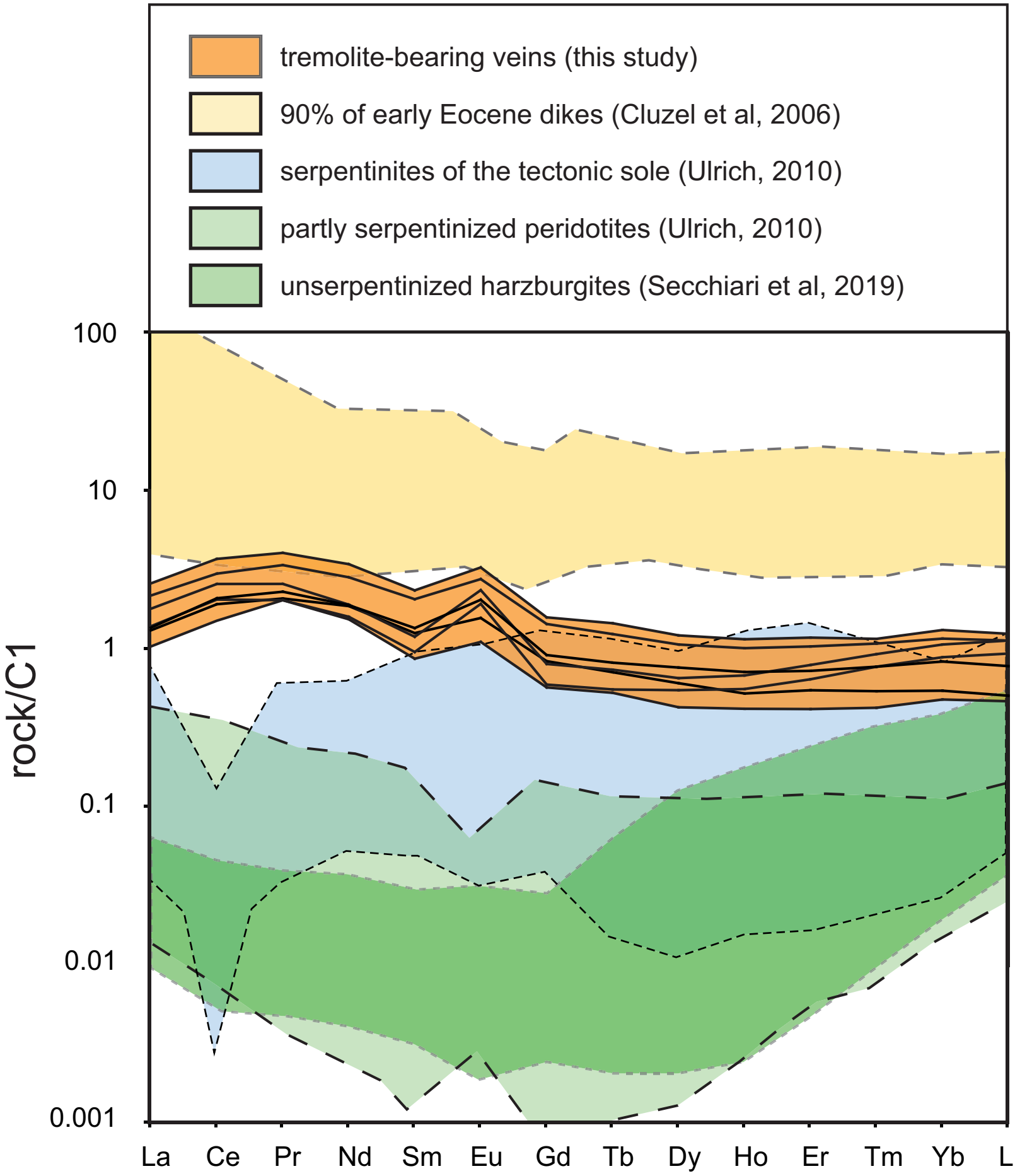

Figure 9

Click here to access/download;Figure;Fig9_LeakeTremolites.eps

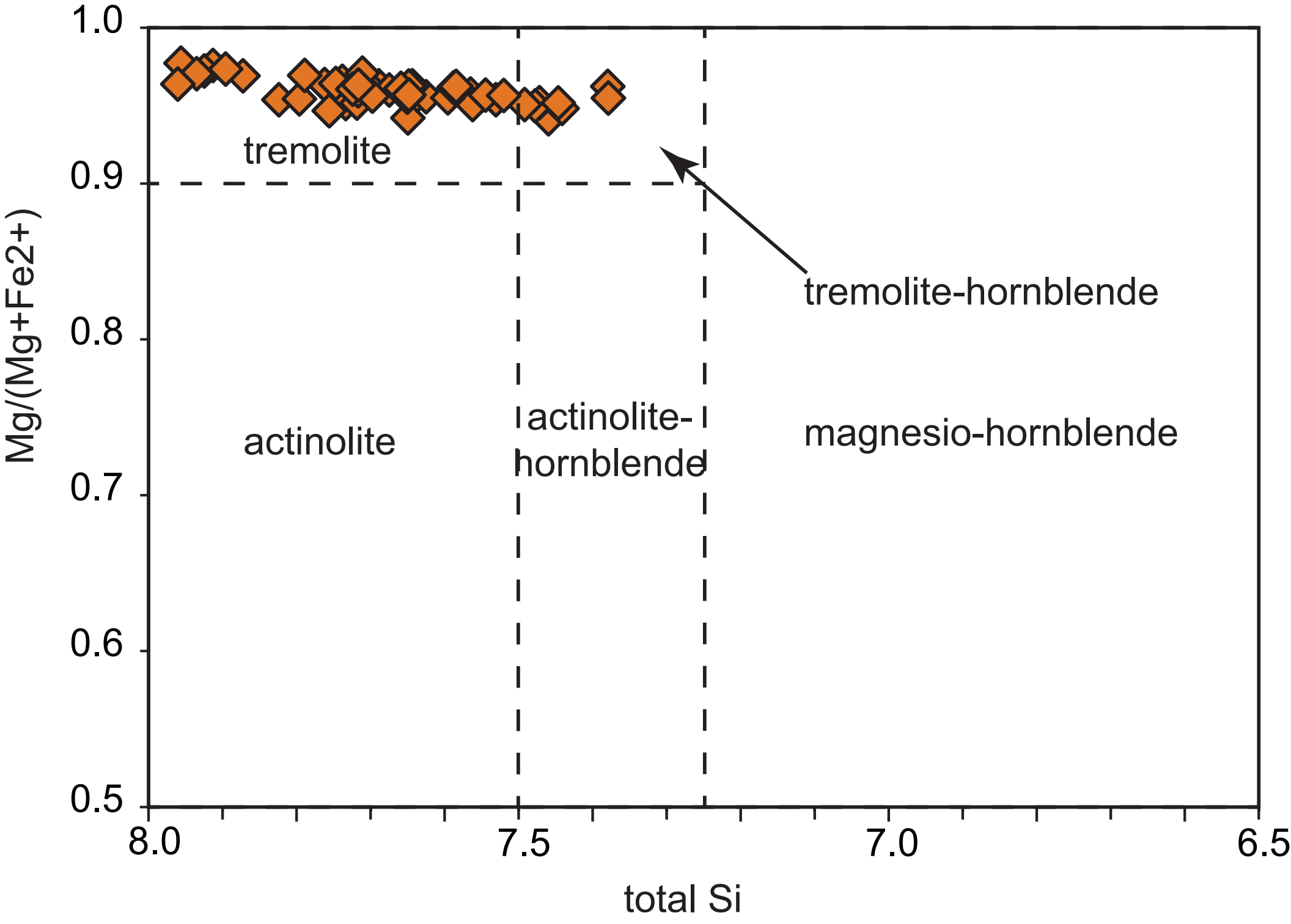

Figure 10

Click here to access/download;Figure;Fig10_CrSi_Tremol.eps

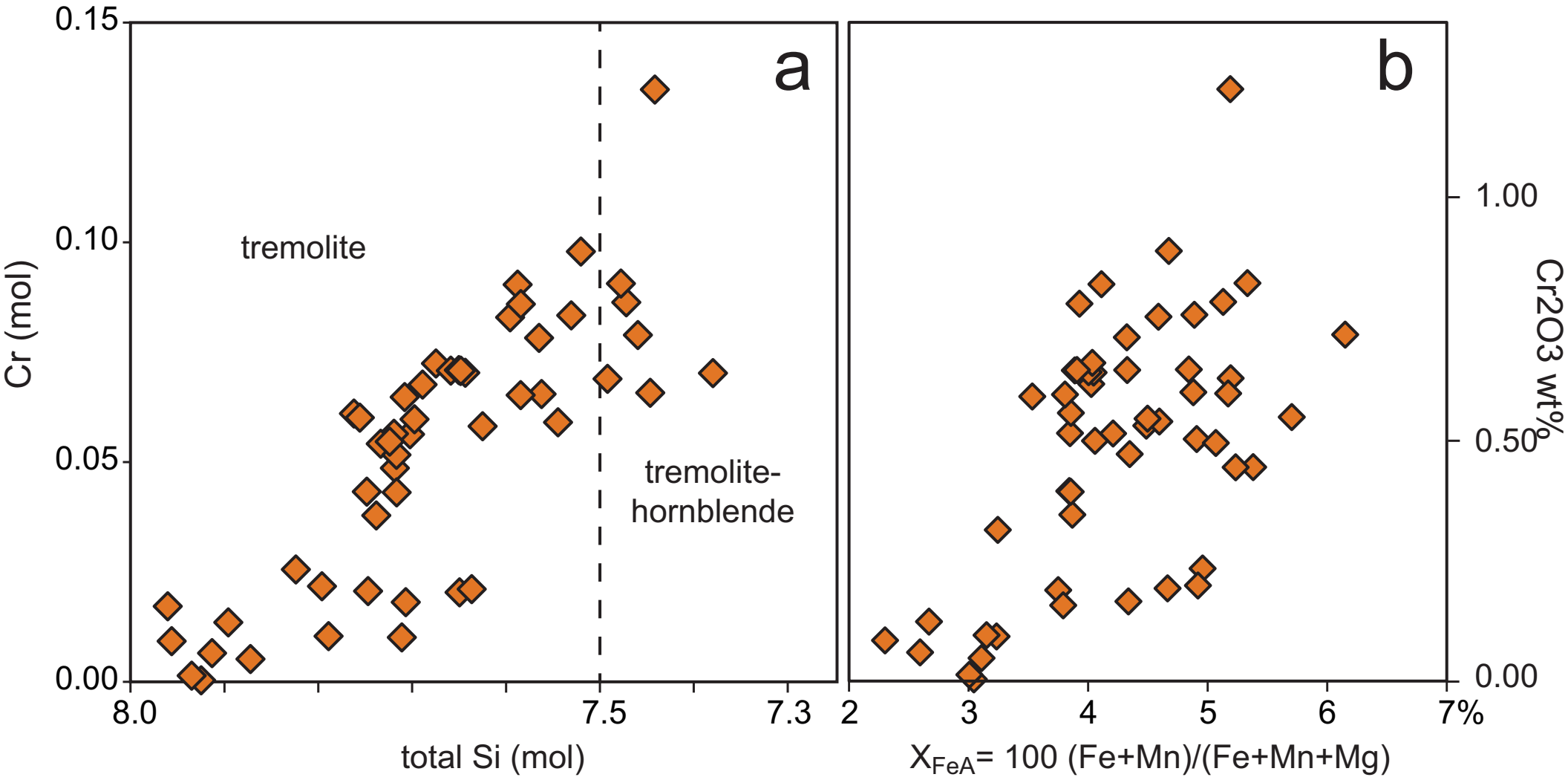

Figure 11

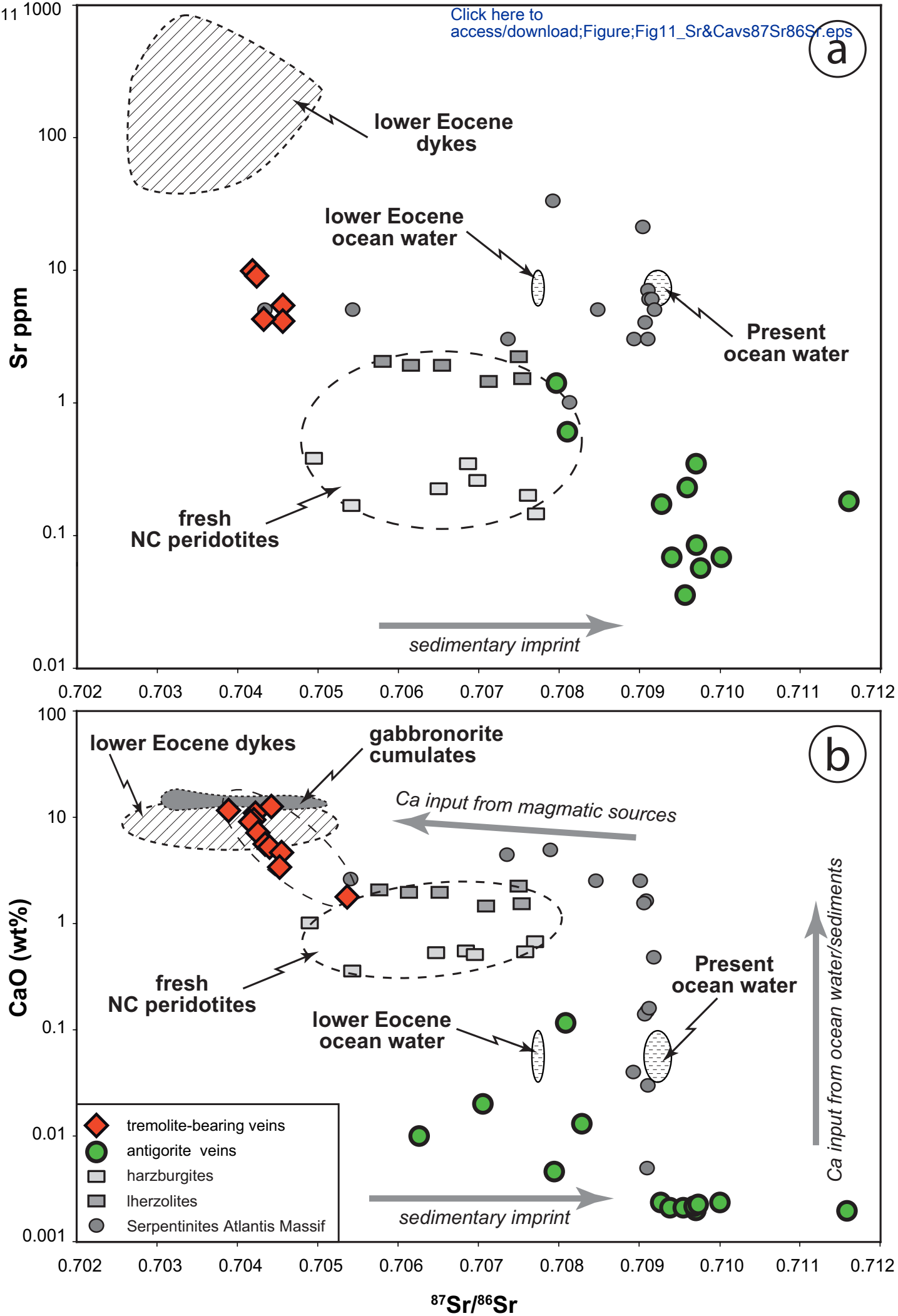

Figure 12

Click here to access/download;Figure;Fig12_IsotOxDeut.eps

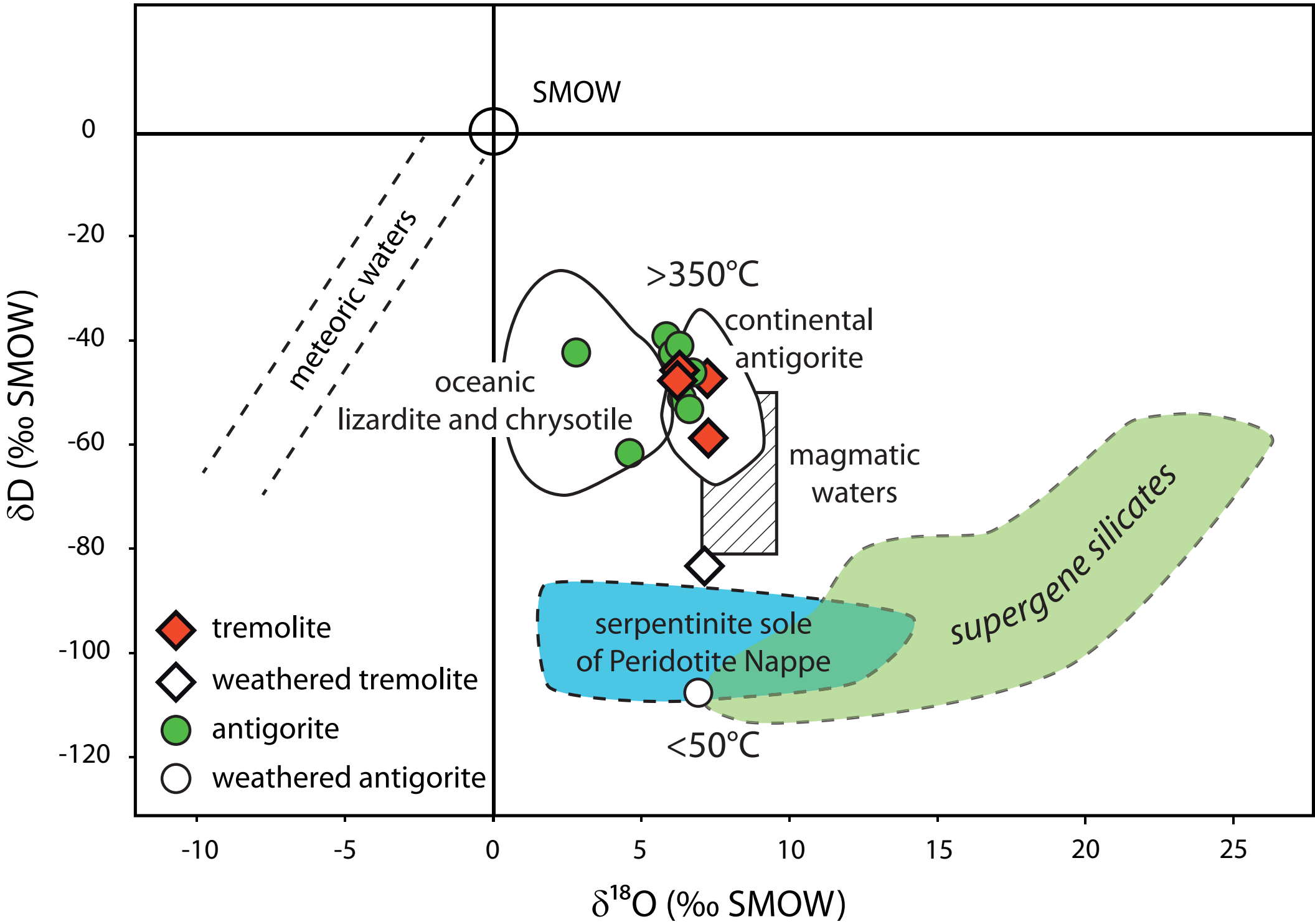

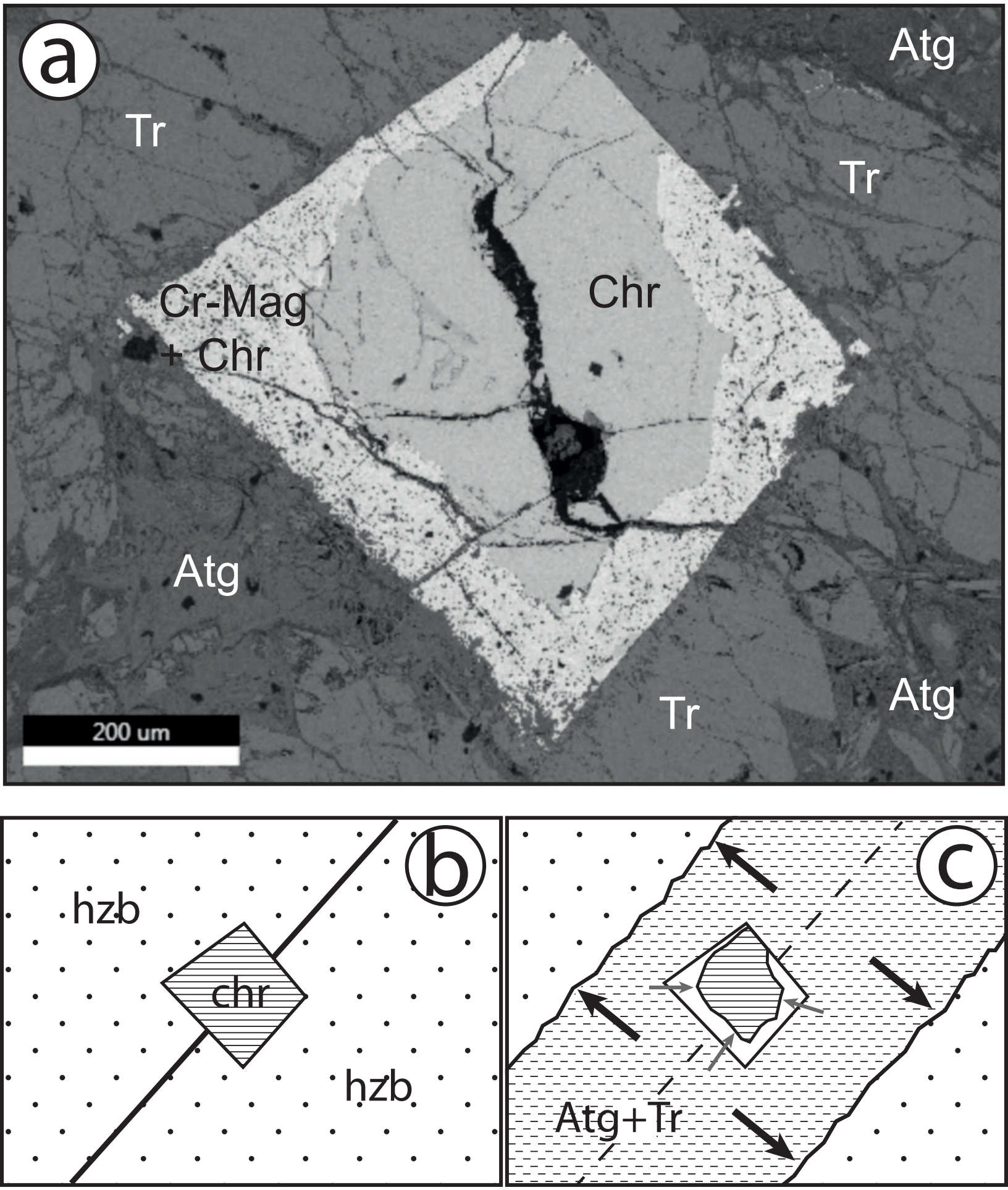

Figure 14